On Mainlobe Orientation of the First- and Second-Order Differential Microphone Arrays

Quansheng Tu and Huawei Chen, *Member, IEEE*

***Abstract*—Due to the increased sensitivity to microphone mismatches, lower-order differential microphone arrays (DMAs) are usually employed in practice, especially the first and second-order DMAs. It is known that the mainlobe orientation of the typical first- and second-order DMAs is both along the fixed endfire direction. This may be no longer true, however, in the presence of microphone mismatchs. This paper studies the fundamental problem of how microphone mismatches affect mainlobe orientation of the first- and second-order DMAs. Some insights into the effects of microphone mismatches on the mainlobe orientation of the two types of DMAs are revealed. In addition, the property on mainlobe orientation of the second-order DMA under ideal condition, which is yet to be known, is also studied. Moreover, tolerance analysis of microphone mismatches to ensure correct mainlobe orientation of the first- and second-order DMAs are performed in order to offer a useful guidance for practical design. Numerical examples are shown to verify the theoretical findings.**

***Index Terms*—Differential microphone array, mainlobe orientation, microphone mismatches, tolerance analysis.**

I. Introduction

DIFFERENTIAL microphone arrays (DMAs) are constructed based on the principle of using the finite-difference of acoustic pressures to closely approximate the spatial derivative of an acoustic pressure field [1]. This construction principle leads to the compact-size nature of DMAs, which is preferable in the practical applications where there is restriction on the size of microphone arrays. In addition, DMAs can achieve higher spatial directivity and frequency-invariant spatial response. These advantages have inspired continuing interest in DMAs [2]–[23].

The spatial directivity of DMAs improves with the order of DMAs increasing. However, it is at the price of the increased sensitivity to sensor mismatches due to white noise amplification [5]. Therefore, lower-order DMAs are usually used in practice, especially the first- and second-order ones. The typical first and second-order DMAs are constructed by two and three closely spaced microphones [1], respectively, and have found a variety of applications. For example, the first-order DMA is used for speech enhancement in [24]–[28], for speech separation in [7], [33], and for sound source localization in [6], [31], [32]. Besides, the first- and second-order DMAs have also served as the fundamental building blocks of other types of DMAs, such as higher-order DMAs [1], [12] or steerable DMAs [9], [19], [29], [30]. For example, third-order DMAs are formed by combinations of two second-order DMAs [1], and first-order steerable DMAs can be constructed by two orthogonal first-order DMAs [9], [19].

It is known that the typical first- and second-order DMAs are end-fire arrays, i.e., their mainlobe is always oriented along the fixed array axis under the ideal condition. As mentioned above, the drawback of DMAs, when compared to conventional additive arrays, is their high sensitivity to sensor mismatches, such as microphone gain and phase mismatches, and sensor self-noise. Then two interesting problems arise: i) How do the microphone mismatches affect mainlobe orientation of the first- and second-order DMAs? ii) What are the tolerances of microphone mismatches to ensure correct mainlobe orientation of the DMAs? This paper aims to address these fundamental problems. The mainlobe orientation of the first- and second-order DMAs in the presence of microphone mismatches is theoretically analyzed.[1] The conditions on the design parameters of the first- and second-order DMAs to guarantee correct mainlobe orientation are derived. In addition, the property on mainlobe orientation of the second-order DMA under ideal condition, which is yet to be known, is also studied. Based on the theoretical analysis, some insights into the effects of microphone mismatches on mainlobe orientation of the first- and second-order DMAs are revealed. Furthermore, to provide a useful guidance for practical design, tolerance analysis of microphone mismatches to ensure correct mainlobe orientation of the first- and second-order DMAs are also performed.

II. Mainlobe Orientation of Ideal First- and Second-Order DMA

A. First-Order DMA

The first-order DMA is constructed with two closely spaced omnidirectional microphones, as shown in Fig. 1(a). Its output is formed through subtracting a delayed version of one microphone signal from the remaining one. Mathematically, for a unit-amplitude harmonic plane-wave impinging on the array with frequency f and incident angle $\theta \in [0^\circ, 360^\circ)$, the received microphone signals can be expressed as

$$S_1 = e^{j\omega t} \tag{1}$$

$$S_2 = e^{j\omega[t-(\tau+d\cos\theta/c)]} \tag{2}$$

Manuscript received May 23, 2019; revised August 17, 2019; accepted August 19, 2019. Date of publication August 27, 2019; date of current version September 11, 2019. This work was supported by the National Natural Science Foundation of China under Grants 61471190 and 61971219. The associate editor coordinating the review of this manuscript and approving it for publication was Dr. Huseyin Hacihabiboglu. *(Corresponding author: Huawei Chen.)*

The authors are with the College of Electronic and Information Engineering, Nanjing University of Aeronautics and Astronautics, Nanjing 210016, China (e-mail: tuquans@nuaa.edu.cn; hwchen@nuaa.edu.cn).

Digital Object Identifier 10.1109/TASLP.2019.2937192

[1]The effects of sensor self-noise on mainlobe orientation of the first- and second-order DMAs are similar to those of microphone gain errors and thus omitted to save pages.

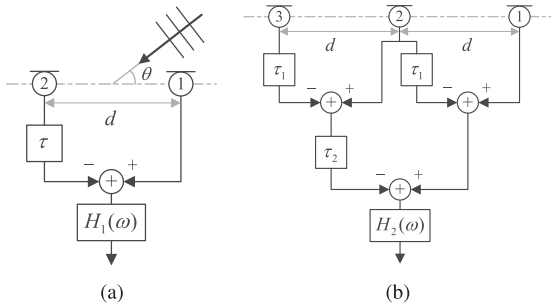

Fig. 1. Array configurations: (a) first-order DMA; (b) second-order DMA.

where $\omega = 2\pi f$, t denotes the time, τ represents the time delay, d refers to the spacing of the microphones, $c \approx 340$ m/s is the speed of the sound in the air, and $j = \sqrt{-1}$.

For a small spacing of microphones ($\omega d/c \ll \pi$), the output of the first-order DMA can be represented as

$$\begin{aligned} E_1(\theta) &= S_1 - S_2 \\ &\approx j\omega(\tau + d\cos\theta/c)e^{j\omega t}. \end{aligned} \tag{3}$$

By compensating the high-pass frequency dependence in (3) using the correction filter $H_1(\omega) = [j\omega(\tau + d/c)]^{-1}$, the beampattern, i.e., normalized array response, of the first-order DMAs can be obtained as

$$\begin{aligned} \overline{E}_1(\theta) &\approx H_1(\omega)E_1(\theta)/e^{j\omega t} \\ &= \alpha + (1-\alpha)\cos\theta \end{aligned} \tag{4}$$

where $\alpha = \tau/(\tau + d/c) \in [0, 1)$.

We can deduce from (4) that the mainlobe orientation of the first-order DMA is always at the desired direction 0°.

B. Second-Order DMA

As shown in Fig. 1(b), the second-order DMA is constructed with three uniformly and closely spaced omnidirectional microphones. The output of the second-order DMA can be seen as being formed by cascading two first-order DMAs with a shared microphone. Suppose the signals received by the first and second microphones are given by (1) and (2), respectively, then the signal by the third microphone can be expressed as

$$S_3 = e^{j\omega[t-(\tau+2d\cos\theta/c)]} \tag{5}$$

For a small spacing of microphones, i.e., $\omega\tau_1 \ll \pi$, $\omega\tau_2 \ll \pi$ and $\omega d/c \ll \pi$, the output of the second-order DMA can be represented as

$$\begin{aligned} E_2(\theta) &= [S_1 - S_2] - e^{-j\omega\tau_2}[S_2 - S_3] \\ &\approx (j\omega)^2(\tau_1 + d/c)(\tau_2 + d/c)[\alpha_1 + (1-\alpha_1)\cos\theta] \\ &\quad \times [\alpha_2 + (1-\alpha_2)\cos\theta]e^{j\omega t} \end{aligned} \tag{6}$$

where

$$\alpha_1 = \tau_1/(\tau_1 + d/c) \tag{7}$$

$$\alpha_2 = \tau_2/(\tau_2 + d/c). \tag{8}$$

By compensating the high-pass frequency dependence in (6) using the correction filter $H_2(\omega) = [(j\omega)^2(\tau_1 + d/c)(\tau_2 + d/c)]^{-1}$, the beampattern of the second-order DMA can be deduced as

$$\begin{aligned} \overline{E}_2(\theta) &\approx H_2(\omega)E_2(\theta)/e^{j\omega t} \\ &= [\alpha_1 + (1-\alpha_1)\cos\theta][\alpha_2 + (1-\alpha_2)\cos\theta]. \end{aligned} \tag{9}$$

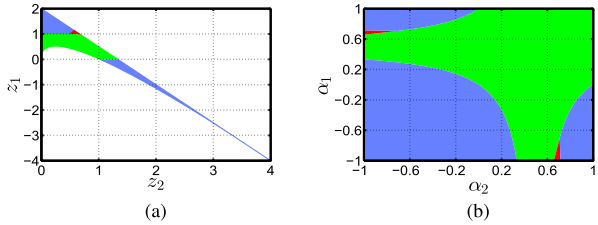

Fig. 2. (Color online) Mainlobe orientation of the ideal second-order DMA versus (a) z_1 and z_2, and (b) α_1 and α_2, where the green, blue, and red areas correspond to the cases with mainlobe orientation of 0°, 180°, and $180^\circ \pm \arccos(\frac{z_1}{2z_2})$, respectively.

For ease of analysis, define

$$z_1 = \alpha_2(1-\alpha_1) + \alpha_1(1-\alpha_2) \tag{10}$$

$$z_2 = (1-\alpha_1)(1-\alpha_2). \tag{11}$$

Then (9) can be rewritten as

$$\overline{E}_2(\theta) \approx (1 - z_1 - z_2) + z_1\cos\theta + z_2\cos^2\theta. \tag{12}$$

This work restricts attention to directivity patterns in the range $\alpha_1 \in (-1, 1)$ and $\alpha_2 \in (-1, 1)$. Note that all standard first- and second-order directivity patterns (cardioid, supercardioid, and hypercardioid) have coefficients in this range [1]. By (10) and (11) we can deduce that z_1 and z_2 should correspondingly satisfy

$$\begin{cases} 0 < z_2 < 4 & \text{(13a)} \\ 2\sqrt{z_2} - 2z_2 \le z_1 < 2 - 3z_2/2. & \text{(13b)} \end{cases}$$

Proposition 1: For an ideal second-order DMA, its mainlobe is oriented toward the desired direction 0°, if z_1 and z_2 satisfy

$$\begin{cases} 2\sqrt{z_2} - 2z_2 \le z_1 \le 1, \quad z_2 \in (0, 1/2) & \text{(14a)} \\ 2\sqrt{z_2} - 2z_2 \le z_1 \le 2\sqrt{2z_2} - 2z_2, \\ \qquad\qquad z_2 \in [1/2, 12 - 8\sqrt{2}) & \text{(14b)} \\ 2\sqrt{z_2} - 2z_2 \le z_1 < 2 - 3z_2/2, \\ \qquad\qquad z_2 \in [12 - 8\sqrt{2}, 1) & \text{(14c)} \\ 0 \le z_1 < 2 - 3z_2/2, \quad z_2 \in [1, 4/3) & \text{(14d)} \end{cases}$$

Otherwise, the mainlobe is oriented toward $180^\circ \pm \arccos(\frac{z_1}{2z_2})$ if $\frac{z_1}{2z_2} \in (-1, 1)$ and $z_1 \ge 2\sqrt{2z_2 + 8z_2^2} - 6z_2$, or the mainlobe is oriented reversely to 180° if not.[2]

The finding in Proposition 1 is shown numerically in Fig. 2. In Fig. 2(a), the mainlobe orientation of the ideal second-order DMA versus the design parameters z_1 and z_2 is shown, where the green, blue, and red areas correspond to the cases with mainlobe orientation of 0°, 180°, and $180^\circ \pm \arccos(\frac{z_1}{2z_2})$, respectively. Alternatively, by mapping z_1 and z_2 to α_1 and α_2 via (10) and (11), the plot of the mainlobe orientation of the ideal second-order DMA versus α_1 and α_2 can be obtained, as shown in Fig. 2(b), where each colored area corresponds to the same-colored one in Fig. 2(a).

To verify the above finding, here we present some numerical examples. Consider the following three second-order DMAs with different design parameters: 1) $\alpha_1 = -0.4082$, $\alpha_2 = 0.4082$ (i.e., $z_1 = 0.33$, $z_2 = 0.83$); 2) $\alpha_1 = 0.2603$, $\alpha_2 = -0.9603$ ($z_1 = -0.20$, $z_2 = 1.45$); and 3) $\alpha_1 = 0.6660$, $\alpha_2 = -0.9460$ ($z_1 = 0.98$, $z_2 = 0.65$). Note that the design parameters for cases 1, 2 and 3 respectively lie in the green, blue and red

[2]The proofs to the propositions hereafter are given in the appendices.

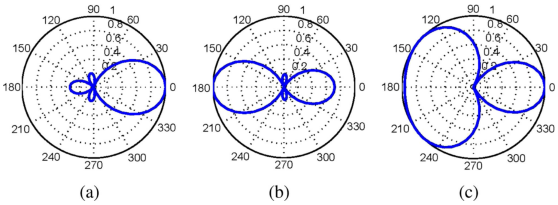

Fig. 3. Beampatterns of the ideal second-order DMAs. (a) $\alpha_1 = -0.4082$, $\alpha_2 = 0.4082$, (b) $\alpha_1 = 0.2603$, $\alpha_2 = -0.9603$, and (c) $\alpha_1 = 0.6660$, $\alpha_2 = -0.9460$, where the mainlobe orientations are at 0°, 180°, and $180^\circ \pm 41.08^\circ$, respectively.

areas in Fig. 2, which implies, according to Proposition 1, that the mainlobes of second-order DMAs for cases 1, 2 and 3 should be oriented toward to 0°, 180°, and $180^\circ \pm \arccos(\frac{z_1}{2z_2}) = 180^\circ \pm 41.08^\circ$ (i.e., 138.92° and 221.08°), respectively. Fig. 3 shows the beampatterns of the three second-order DMAs.[3] As can be seen from Fig. 3, the mainlobes orientations of the second-order DMAs are indeed consistent with those derived by the theoretical analysis.

III. Effects of Microphone Mismatches on Mainlobe Orientation of First-Order DMA

A. Effect of Microphone Gain Errors

In the presence of microphone gain errors, the received microphone signals of the first-order DMA can be modeled as

$$S_1^{(g)} = \eta_1 e^{j\omega t} \tag{15}$$

$$S_2^{(g)} = \eta_2 e^{j\omega[t-(\tau+d\cos\theta/c)]} \tag{16}$$

where $\eta_1 = 1-\varepsilon_1$ and $\eta_2 = 1-\varepsilon_2$, with ε_1 and ε_2 being the gain errors of the first and second microphones, respectively.

For a small spacing of microphones, the output of the first-order DMA is given by

$$\begin{aligned} E_1^{(g)}(\theta) &= S_1^{(g)} - S_2^{(g)} \\ &\approx \{j\eta_2\omega(\tau + d/c)[\alpha + (1-\alpha)\cos\theta] \\ &\quad + (\eta_1 - \eta_2)\}e^{j\omega t}. \end{aligned} \tag{17}$$

Accordingly, by compensating the high-pass frequency dependence in (17) using the correction filter $H_1(\omega) = [j\omega(\tau + d/c)]^{-1}$, the beampattern of the first-order DMA with microphone gain errors now becomes

$$\begin{aligned} \overline{E}_1^{(g)}(\theta) &\approx H_1(\omega)E_1^{(g)}(\theta)/e^{j\omega t} \\ &= \eta_2[\alpha + (1-\alpha)\cos\theta] + (\eta_1 - \eta_2)(1-\alpha)/(j\Omega). \end{aligned} \tag{18}$$

where $\Omega = \omega d/c$.

Proposition 2: The mainlobe orientation of the first-order DMA is independent of microphone gain errors and always at the desired direction.

Remark 1: The microphone gain errors have no effect on the mainlobe orientation of the first-order DMAs. This is unlike the steerable first-order DMA [16], which are constructed by two orthogonal first-order DMAs. Microphone gain errors can lead to noticeable bias in mainlobe orientation of the steerable first-order DMA, since its mainlobe orientation depends on microphone gain errors. In contrast, there is no such noticeable bias in the mainlobe orientation of the first-order DMA.

[3]We would like to point out that, although approximated models have been used in theoretical analysis throughout the paper, all the beampatterns hereafter are based on the rigorous models instead of the approximated ones. Moreover, all the beampatterns hereafter are normalized to facilitate comparison.

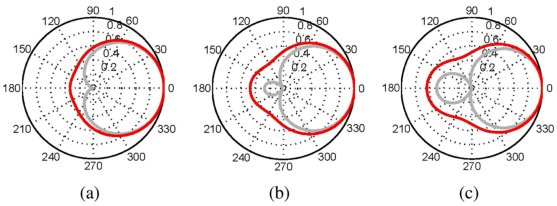

Fig. 4. Beampatterns of the first-order DMAs with microphone gain errors (in red lines). (a) $\alpha = 0.5$ (cardioid), (b) $\alpha = 0.3660$ (supercardioid), and (c) $\alpha = 0.25$ (hypercardioid), where $\Omega = \pi/36$ rad., $\eta_1 = -0.2646$ dB and $\eta_2 = 0.2567$ dB. For comparison, the beampatterns without gain errors are also shown (in gray lines). The mainlobe orientations with gain errors are all at 0°.

As a numerical example, Fig. 4 plots the beampatterns of three typical first-order DMAs with microphone gain errors (in red lines), i.e., $\alpha = 0.5$ (cardioid), $\alpha = 0.3660$ (supercardioid), and $\alpha = 0.25$ (hypercardioid), where $\Omega = \pi/36$ rad., $\eta_1 = -0.2646$ dB and $\eta_2 = 0.2567$ dB. For comparison, the corresponding beampatterns without microphone gain errors are also plotted in Fig. 4 (in gray lines). From Fig. 4 we can see that the mainlobes of the three first-order DMAs are all oriented towards 0°, i.e., there is no noticeable bias in the mainlobe orientation, as revealed by the theoretical analysis.

B. Effect of Microphone Phase Errors

In the presence of microphone phase errors, the received microphone signals of the first-order DMA can be expressed as

$$S_1^{(p)} = e^{j[\omega t + \psi_1]} \tag{19}$$

$$S_2^{(p)} = e^{j[\omega t - \omega(\tau + d\cos\theta/c) + \psi_2]} \tag{20}$$

where ψ_1 and ψ_2 denote the phase errors of the first and second microphones, respectively.

For small microphone phase errors, it follows that $\cos(\psi_1 - \psi_2) \approx 1$ and $\sin(\psi_1 - \psi_2) \approx \psi_1 - \psi_2$. Then, the output of the first-order DMA can be reduced to

$$\begin{aligned} E_1^{(p)}(\theta) &= S_1^{(p)} - S_2^{(p)} \\ &\approx j\omega(\tau + d/c)[\alpha + (1-\alpha)\cos\theta \\ &\quad + c(1-\alpha)(\psi_1 - \psi_2)/(\omega d)]\, e^{j\omega t}. \end{aligned} \tag{21}$$

By (21), the beampattern of the first-order DMA with microphone phase errors can be deduced as

$$\begin{aligned} \overline{E}_1^{(p)}(\theta) &\approx H_1(\omega)E_1^{(p)}(\theta)/e^{j\omega t} \\ &= \alpha + (1-\alpha)\cos\theta + (1-\alpha)(\psi_1 - \psi_2)/\Omega. \end{aligned} \tag{22}$$

Proposition 3: The mainlobe orientation of the first-order DMA is dependent on microphone phase errors and along the end-fire directions. Specifically, if $\psi_1 \geq \psi_2$ or if $\psi_1 < \psi_2$ with $\frac{\psi_1 - \psi_2}{\psi_1 - \psi_2 - \Omega} \triangleq \alpha_T \leq \alpha$, then the mainlobe orientation is at 0°; otherwise, the mainlobe orientation is at 180°.

Remark 2: Unlike the effect of microphone gain errors, microphone phase errors may result in a severe problem for mainlobe orientation of the first-order DMA. If the design parameter α is not chosen appropriately, particularly for small-valued α, the mainlobe orientation will be reversed to the opposite of the desired direction, i.e., 180°. Moreover, the detrimental effect is more pronounced in lower frequencies or for smaller array sizes. This finding is helpful to better understand the mainlobe

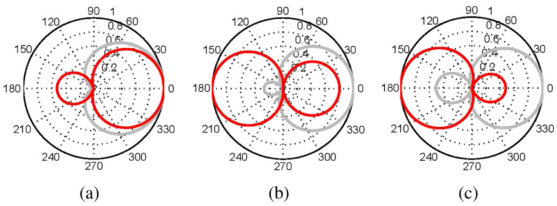

Fig. 5. Beampatterns of the first-order DMAs with microphone phase errors (in red lines). (a) $\alpha = 0.5$ (cardioid), (b) $\alpha = 0.3660$ (supercardioid), and (c) $\alpha = 0.25$ (hypercardioid), where $\Omega = \pi/36$ rad., $\psi_1 = -1.72^\circ$ and $\psi_2 = 1.72^\circ$. For comparison, the beampatterns without phase errors are also shown (in gray lines). The mainlobe orientations with phase errors for (a), (b) and (c) are at 0°, 180° and 180°, respectively.

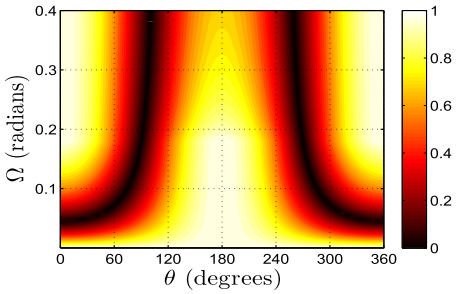

Fig. 6. Beampattern of the first-order hypercardioid DMA with microphone phase errors as a function of Ω and θ, where $\psi_1 = -1.72^\circ$ and $\psi_2 = 1.72^\circ$.

orientation reversal problem of the steerable first-order DMA due to microphone phase errors [16], i.e., it is actually because the basic building blocks of steerable first-order DMA, the first-order DMA, suffer from the problem.

Remark 3: Similar to the effect of microphone gain errors, there is also no noticeable bias in the mainlobe orientation when it is around the desired direction 0°. By combining the analysis of the effects of microphone gain and phase errors, we can conclude that the mainlobe orientation of the first-order DMA is only along the endfire directions (0° or 180°), i.e., along array axis, in the presence of microphone mismatches.

Fig. 5 shows the beampatterns of the three typical first-order DMAs with cardioid, supercardioid and hypercardioid responses in the presence of microphone phase errors (in red lines), where $\Omega = \pi/36$ rad., $\psi_1 = -1.72^\circ$ and $\psi_2 = 1.72^\circ$. For comparison, the corresponding beampatterns without microphone phase errors are also shown in Fig. 5 (in gray lines). As per Proposition 3, for this example we have $\alpha_T = 0.4074$. It follows that the mainlobe orientation is at 0° when $\alpha \geq 0.4074$, otherwise the mainlobe orientation will be reversed to 180°. In this example, the design parameters of the first-order DMAs with supercardioid and hypercardioid responses are both less than 0.4074, therefore we can see that their mainlobe orientations are reversed to 180°. Comparatively, for the case with cardioid response, its design parameter is larger than 0.4074, thus its mainlobe is oriented correctly at 0°, where there is no noticeable orientation bias as pointed out previously.

Fig. 6 shows the beampattern of the first-order hypercardioid DMA with microphone phase errors as a function of Ω and θ, where $\psi_1 = -1.72^\circ$ and $\psi_2 = 1.72^\circ$. Recall that Ω is proportional to frequency f and array size d. It can be seen from Fig. 6 that, with the decreasing of Ω, i.e., the decreasing of frequency or array size, the mainlobe orientation tends to be reversed to 180° from the desired direction 0°. This is consistent with the theoretical finding that the effect of microphone phase errors is more pronounced in lower frequencies or for smaller array size.

TABLE I
MICROPHONE PHASE-ERROR TOLERANCES FOR THE FIRST-ORDER DMAS WITH FREQUENCY BAND [200, 3700] HZ

DMA type	$d = 1$ cm	$d = 2$ cm
first-order cardioid	$\Delta_\psi \leq 1.0588^\circ$	$\Delta_\psi \leq 2.1176^\circ$
first-order supercardioid	$\Delta_\psi \leq 0.6113^\circ$	$\Delta_\psi \leq 1.2226^\circ$
first-order hypercardioid	$\Delta_\psi \leq 0.3529^\circ$	$\Delta_\psi \leq 0.7059^\circ$

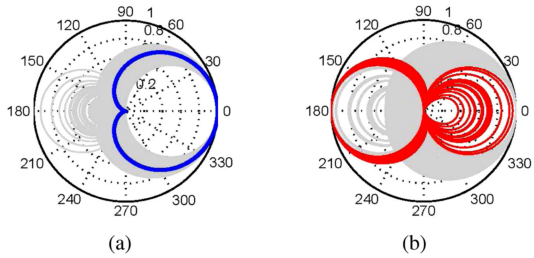

Fig. 7. Beampatterns of the first-order cardioid DMA with varying microphone phase errors, where $d = 0.01$ m and $f \in [200, 3700]$ Hz. (a) $|\psi_i| \leq 1.0588^\circ$; (b) $|\psi_i| \leq 1.6318^\circ$, where the beampatterns with abnormal orientation are highlighted in red lines, and the ideal beampattern is also shown in blue line.

IV. MICROPHONE MISMATCH TOLERANCE ANALYSIS FOR CORRECT MAINLOBE ORIENTATION OF FIRST-ORDER DMA

As discussed in the above section, microphone mismatch may lead to the problem of mainlobe orientation reversal for a first-order DMA. Therefore, it is of practical interest to know the tolerance of microphone mismatch for ensuring the correct mainlobe orientation of the first-order DMA. Recall that for a first-order DMA, microphone gain errors have no effect on the mainlobe orientation. It suffices to discuss the tolerance of microphone phase errors.

We summarize our result in the following proposition:

Proposition 4: Given the design specification of a first-order DMA, i.e., the array size d, the working frequency band $[f_l, f_h]$ and the design parameter α, to guarantee the mainlobe orientation is always at 0°, the tolerance of microphone phase errors should satisfy $\Delta_\psi \leq \frac{\pi f_l d \alpha}{c(1-\alpha)}$.

For the typical speech communication applications with the frequency band of [200, 3700] Hz, the corresponding tolerances of microphone phase errors for the three popular first-order DMAs, i.e., cardioid, supercardioid and hypercardioid, are shown in Table I, which are derived with the help of Proposition 4. Note that the maximum of the necessary phase deviation is below the specifications of typical MEMS microphones, see, for example, [34] and [35].

Here we present some numerical examples to evaluate the derived results. Figs. 7–9 show the beampatterns of the three first-order DMAs with an array size of 0.01 m under varying microphone phase errors. For each figure, 200 trials are carried out at each of the five distinct frequencies uniformly spaced in [200, 3700] Hz, i.e., totally 1000 trials. It can be seen from Figs. 7(a), 8(a) and 9(a) that the mainlobes are all correctly oriented at 0° since the microphone phase errors are within the maximum tolerances. However, when the maximum tolerances of microphone phase errors are violated, the mainlobe orientation reversal problem occurs as shown in Figs. 7(b), 8(b) and 9(b), where the beampatterns with abnormal mainlobe orientation have been highlighted in red.

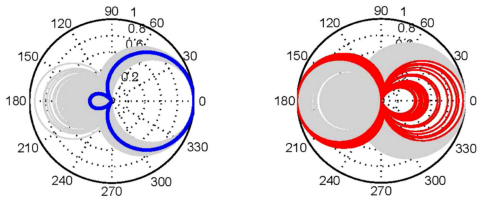

(a) (b)

Fig. 8. Beampatterns of the first-order supercardioid DMA with varying microphone phase errors, where $d = 0.01$ m and $f \in [200, 3700]$ Hz. (a) $|\psi_i| \le 0.6113°$; (b) $|\psi_i| \le 1.1843°$, where the beampatterns with abnormal orientation are highlighted in red lines, and the ideal beampattern is also shown in blue line.

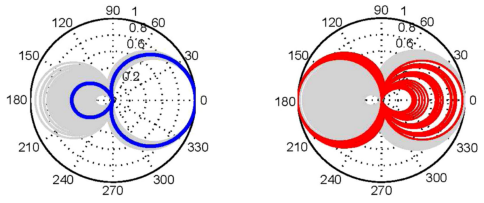

(a) (b)

Fig. 9. Beampatterns of the first-order hypercardioid DMA with varying microphone phase errors, where $d = 0.01$ m and $f \in [200, 3700]$ Hz. (a) $|\psi_i| \le 0.3529°$; (b) $|\psi_i| \le 0.9259°$, where the beampatterns with abnormal orientation are highlighted in red lines, and the ideal beampattern is also shown in blue line.

V. Effects of Microphone Mismatches on Mainlobe Orientation of Second-Order DMA

A. Effect of Microphone Gain Errors

Denote by (15) and (16) the signals received by the first and second microphones of the second-order DMA with microphone gain errors, respectively. Then, the received signal at the third microphone can be modeled as

$$S_3^{(g)} = \eta_3 e^{j\omega[t-(\tau+2d\cos\theta/c)]} \tag{23}$$

where $\eta_3 = 1 - \varepsilon_3$, with ε_3 denoting the gain error of the third microphone.

With (15), (16) and (23), the output signal of the second-order DMA can be written as

$$\begin{aligned} E_2^{(g)}(\theta) &= [S_1^{(g)} - S_2^{(g)}] - e^{-j\omega\tau_2}[S_2^{(g)} - S_3^{(g)}] \\ &\approx \{\eta_1 - 2\eta_2 + \eta_3 + j\omega(\eta_2 - \eta_3)(\tau_1 + d/c) \\ &\quad \times [\alpha_1 + (1-\alpha_1)\cos\theta] + j\omega(\eta_2 - \eta_3)(\tau_2 + d/c) \\ &\quad \times [\alpha_2 + (1-\alpha_2)\cos\theta] - \eta_3\omega^2(\tau_1 + d/c)(\tau_2 + d/c) \\ &\quad \times [\alpha_1 + (1-\alpha_1)\cos\theta][\alpha_2 + (1-\alpha_2)\cos\theta]\}e^{j\omega t}. \end{aligned} \tag{24}$$

By (24), the beampattern of the second-order DMA with microphone gain errors can be derived as

$$\begin{aligned} &\overline{E}_2^{(g)}(\theta) \\ &\approx H_2(\omega)E_2^{(g)}(\theta)/e^{j\omega t} \\ &= \eta_3(1 - z_1 - z_2) + z_1\left[\eta_3\cos\theta - \frac{j(\eta_2 - \eta_3)}{\Omega}\right] \\ &\quad + z_2\left[\frac{2\eta_2 - \eta_1 - \eta_3}{\Omega^2} - \frac{2j(\eta_2 - \eta_3)\cos\theta}{\Omega} + \eta_3\cos^2\theta\right]. \end{aligned} \tag{25}$$

Proposition 5: The mainlobe orientation of the second-order DMA is dependent of the microphone gain errors. Denote

$$G(\eta_i, \Omega) = (2\eta_2^2 - 2\eta_2\eta_3 + \eta_3^2 - \eta_1\eta_3)/(\eta_3^2\Omega^2). \tag{26}$$

Then we have:

1) The mainlobe orientation is at $0°$ if the following conditions hold

1.1) For $G(\eta_i, \Omega) \ge 0$,

$$\begin{cases} 2\sqrt{z_2} - 2z_2 \le z_1 \le 1, & z_2 \in (0, 1/2) \quad (27a) \\ 2\sqrt{z_2} - 2z_2 \le z_1 \le 2\sqrt{2z_2} - 2z_2, & \\ \qquad z_2 \in [1/2, 12 - 8\sqrt{2}) \quad (27b) \\ 2\sqrt{z_2} - 2z_2 \le z_1 < 2 - 3z_2/2, & z_2 \in [12 - 8\sqrt{2}, 1) \quad (27c) \\ 0 \le z_1 < 2 - 3z_2/2, & z_2 \in [1, 4/3) \quad (27d) \end{cases}$$

1.2) For $-7/32 \le G(\eta_i, \Omega) < 0$,

$$\begin{cases} 2\sqrt{z_2} - 2z_2 \le z_1 \le 1 + z_2 G(\eta_i, \Omega), & \\ \qquad z_2 \in \left(0, \frac{1}{2 - G(\eta_i, \Omega)}\right) & (28a) \\ 2\sqrt{z_2} - 2z_2 \le z_1 \le 2\sqrt{2z_2 + 2z_2^2 G(\eta_i, \Omega)} - 2z_2, & \\ \qquad z_2 \in \left[\frac{1}{2 - G(\eta_i, \Omega)}, \frac{12 - 8\sqrt{2 + 8G(\eta_i, \Omega)}}{1 - 32G(\eta_i, \Omega)}\right) & (28b) \\ 2\sqrt{z_2} - 2z_2 \le z_1 < 2 - 3z_2/2, & \\ \qquad z_2 \in \left[\frac{12 - 8\sqrt{2 + 8G(\eta_i, \Omega)}}{1 - 32G(\eta_i, \Omega)}, 1\right) & (28c) \\ 0 \le z_1 < 2 - 3z_2/2, \quad z_2 \in \left[1, \frac{4}{3}\right) & (28d) \end{cases}$$

1.3) For $-1/4 \le G(\eta_i, \Omega) < -7/32$,

$$\begin{cases} 2\sqrt{z_2} - 2z_2 \le z_1 \le 1 + z_2 G(\eta_i, \Omega), & \\ \qquad z_2 \in \left(0, \frac{1}{2 - G(\eta_i, \Omega)}\right) & (29a) \\ 2\sqrt{z_2} - 2z_2 \le z_1 \le 2\sqrt{2z_2 + 2z_2^2 G(\eta_i, \Omega)} - 2z_2, & \\ \qquad z_2 \in \left[\frac{1}{2 - G(\eta_i, \Omega)}, 1\right) & (29b) \\ 0 \le z_1 \le 2\sqrt{2z_2 + 2z_2^2 G(\eta_i, \Omega)} - 2z_2, & \\ \qquad z_2 \in \left[1, \frac{12 - 8\sqrt{2 + 8G(\eta_i, \Omega)}}{1 - 32G(\eta_i, \Omega)}\right) & (29c) \\ 0 \le z_1 < 2 - 3z_2/2, & \\ \qquad z_2 \in \left[\frac{12 - 8\sqrt{2 + 8G(\eta_i, \Omega)}}{1 - 32G(\eta_i, \Omega)}, \frac{4}{3}\right) & (29d) \end{cases}$$

1.4) For $-1/2 \le G(\eta_i, \Omega) < -1/4$,

$$\begin{cases} 2\sqrt{z_2} - 2z_2 \le z_1 \le 1 + z_2 G(\eta_i, \Omega), & \\ \qquad z_2 \in \left(0, \frac{1}{2 - G(\eta_i, \Omega)}\right) & (30a) \\ 2\sqrt{z_2} - 2z_2 \le z_1 \le 2\sqrt{2z_2 + 2z_2^2 G(\eta_i, \Omega)} - 2z_2, & \\ \qquad z_2 \in \left[\frac{1}{2 - G(\eta_i, \Omega)}, 1\right) & (30b) \\ 0 \le z_1 \le 2\sqrt{2z_2 + 2z_2^2 G(\eta_i, \Omega)} - 2z_2, & \\ \qquad z_2 \in \left[1, \frac{2}{1 - 2G(\eta_i, \Omega)}\right] & (30c) \end{cases}$$

1.5) For $-2 \le G(\eta_i, \Omega) < -1/2$,

$$\begin{cases} 2\sqrt{z_2} - 2z_2 \le z_1 \le 1 + z_2 G(\eta_i, \Omega), & \\ \qquad z_2 \in \left(0, \frac{1}{2 - G(\eta_i, \Omega)}\right) & (31a) \\ 2\sqrt{z_2} - 2z_2 \le z_1 \le 2\sqrt{2z_2 + 2z_2^2 G(\eta_i, \Omega)} - 2z_2, & \\ \qquad z_2 \in \left[\frac{1}{2 - G(\eta_i, \Omega)}, -\frac{1}{2G(\eta_i, \Omega)}\right] & (31b) \end{cases}$$

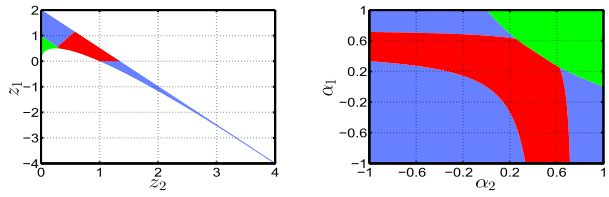

(a) (b)

Fig. 10. (Color online) Mainlobe orientation of the second-order DMA with microphone gain errors versus (a) z_1 and z_2, and (b) α_1 and α_2, where $\eta_1 = 0.0260$ dB, $\eta_2 = -0.0261$ dB, $\eta_3 = 0.0260$ dB, and $\Omega = \pi/36$ rad. The green, blue, and red areas correspond to the cases with mainlobe orientation of 0°, 180°, and $180^\circ \pm \arccos(\frac{z_1}{2z_2})$, respectively.

1.6) For $G(\eta_i, \Omega) < -2$,

$$2\sqrt{z_2} - 2z_2 \le z_1 \le 1 + z_2 G(\eta_i, \Omega),$$
$$z_2 \in \left(0, \frac{-2\sqrt{-1 - G(\eta_i, \Omega)} - G(\eta_i, \Omega)}{(2 + G(\eta_i, \Omega))^2}\right] \qquad (32)$$

2) If (27)–(32) do not hold, then the mainlobe orientation is around $180^\circ \pm \arccos(\frac{z_1}{2z_2})$ when $\frac{z_1}{2z_2} \in (-1, 1)$ and $z_1 \ge 2\sqrt{2z_2[1 + (4 + G(\eta_i, \Omega))z_2]} - 6z_2$, or the mainlobe is oriented reversely to 180° when not.

Regarding the effects of microphone gain errors on the second-order DMA, we have the following remarks.

Remark 4: Recall that microphone gain errors have no effect on the mainlobe orientation of the first-order DMA. However, this is no longer the case for the second-order DMA. Microphone gain errors may have a negative effect on the second-order DMA, and can lead to its mainlobe orientation being reversed to 180° or somewhere far away from the desired direction, even though the mainlobe is correctly oriented under the condition of no microphone gain errors. Moreover, this negative effect of microphone gain errors is more significant in lower frequencies or for smaller array sizes.

Remark 5: The possible mainlobe orientation of the second-order DMAs with microphone gain errors is only around the specific angles, i.e., 0°, 180° or $180^\circ \pm \arccos(\frac{z_1}{2z_2})$, which are independent on the microphone gain errors, and are also the same as in the case of no microphone gain errors. Moreover, this is unlike the first-order DMA, whose mainlobe orientation is only along the endfire directions under the impact of microphone mismatch errors.

Remark 6: In the presence of microphone gain errors, there will be no noticeable bias in the mainlobe orientation of the second-order DMA, i.e., its mainlobe will be oriented to the desired direction without any noticeable bias if the design parameter α_1 and α_2 are appropriately set. This effect is similar to that for the first-order DMA.

Now we present some numerical examples to illustrate the findings. Suppose the microphone gain errors $\eta_1 = 0.0260$ dB, $\eta_2 = -0.0261$ dB, $\eta_3 = 0.0260$ dB, and $\Omega = \pi/36$ rad. As per Proposition 5, Fig. 10(a) shows the mainlobe orientation of the second-order DMA versus z_1 and z_2, where the green, blue, and red areas correspond to the cases with mainlobe orientation of 0°, 180°, and $180^\circ \pm \arccos(\frac{z_1}{2z_2})$, respectively. By the mapping relationship (10) and (11), we can obtain the corresponding mainlobe orientation of the second-order DMA as a function of the design parameters α_1 and α_2, shown in Fig. 10(b).

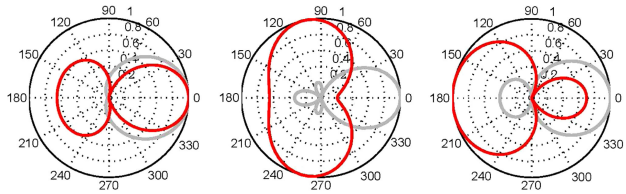

(a) (b) (c)

Fig. 11. Beampatterns of the second-order DMA with microphone gain errors (in red lines). (a) $\alpha_1 = 0.5000$, $\alpha_2 = 0.5000$ (cardioid), (b) $\alpha_1 = 0.4082$, $\alpha_2 = -0.4082$ (hypercardioid), and (c) $\alpha_1 = 0.0418$, $\alpha_2 = 0.7182$, where $\Omega = \pi/36$ rad., $\eta_1 = 0.0260$ dB, $\eta_2 = -0.0261$ dB, $\eta_3 = 0.0260$ dB. For comparison, the beampatterns without gain errors are also shown (in gray lines). The mainlobe orientations with gain errors for (a), (b), and (c) are at 0°, $180^\circ \pm 78.46^\circ$, and 180°, respectively.

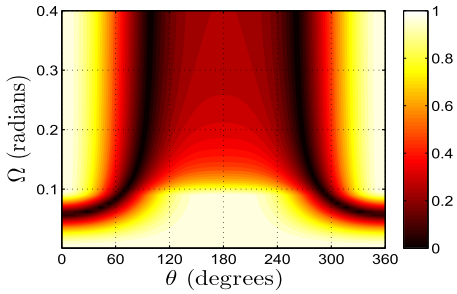

Fig. 12. Beampattern of the second-order DMA ($\alpha_1 = 0.0418$, $\alpha_2 = 0.7182$) with microphone gain errors as a function of Ω and θ, where $\eta_1 = 0.0260$ dB, $\eta_2 = -0.0261$ dB, $\eta_3 = 0.0260$ dB.

Figs. 11(a), 11(b), and 11(c) show the beampatterns of three second-order DMAs with $\alpha_1 = 0.5000$, $\alpha_2 = 0.5000$; $\alpha_1 = 0.4082$, $\alpha_2 = -0.4082$; and $\alpha_1 = 0.0418$, $\alpha_2 = 0.7182$, respectively, under the above-specified microphone gain errors. The first two are well-known DMAs with second-order cardioid and hypercardioid responses. For comparison, the corresponding beampatterns without microphone gain errors are also shown in the figures. Note that the design parameters α_1 and α_2 for Figs. 11(a), 11(b), and 11(c) are located in the green, red, and blue areas in Fig. 10(b), respectively. It means, according to Proposition 5, that the mainlobe orientations of the three second-order DMAs should be theoretically at 0°, $180^\circ \pm \arccos(\frac{z_1}{2z_2}) = 180^\circ \pm 78.46^\circ$, 180°, respectively. As can be seen from Fig. 11, the theoretically predicted mainlobe orientations agree well with those in the simulation results. Note that, for the second-order cardioid DMA in Fig. 11(a), its mainlobe is oriented around the desired direction, and indeed there is no noticeable error in the mainlobe orientation.

Fig. 12 shows the beampattern of the second-order DMA with microphone gain errors as a function of Ω and θ, where the simulation conditions are similar to those in Fig. 11(c). From Fig. 12 we can clearly see that the mainlobe orientation of the second-order DMA deteriorates greatly for smaller value of Ω, i.e., for lower frequencies or smaller array sizes, which is consistent with the theoretical finding.

B. Effect of Microphone Phase Errors

Assume that the received signals at microphones 1 and 2 of the second-order DMA with microphone phase errors are given by (19) and (20), respectively. Then, the received signal

at microphone 3 can be modeled as

$$S_3^{(p)} = e^{j[\omega t-\omega(\tau+2d\cos\theta/c)+\psi_3]} \tag{33}$$

By (19), (20) and (33), the output signal of the second-order DMA can be expressed as

$$\begin{aligned} E_2^{(p)}(\theta) &= [S_1^{(p)} - S_2^{(p)}] - e^{-j\omega\tau_2}[S_2^{(p)} - S_3^{(p)}] \\ &\approx \{e^{j\psi_1} - 2e^{j\psi_2} + e^{j\psi_3} + j\omega(e^{j\psi_2} - e^{j\psi_3}) \\ &\quad \times \{(\tau_1 + d/c)[\alpha_1 + (1-\alpha_1)\cos\theta] \\ &\quad + (\tau_2 + d/c)[\alpha_2 + (1-\alpha_2)\cos\theta]\} \\ &\quad - \omega^2 e^{j\psi_3}(\tau_1 + d/c)(\tau_2 + d/c) \\ &\quad \times [\alpha_1 + (1-\alpha_1)\cos\theta][\alpha_2 + (1-\alpha_2)\cos\theta]\}e^{j\omega t}. \end{aligned} \tag{34}$$

Accordingly, the beampattern of the second-order DMA with microphone phase errors is given by

$$\begin{aligned} \overline{E}_2^{(p)}(\theta) &\approx H_2(\omega)E_2^{(p)}(\theta)/e^{j\omega t} \\ &= e^{j\psi_3}(1 - z_1 - z_2) + z_1\left[\cos\theta - \frac{j(e^{j\psi_2} - e^{j\psi_3})}{\Omega}\right] \\ &\quad + z_2\left[\frac{2e^{j\psi_2} - e^{j\psi_1} - e^{j\psi_3}}{\Omega^2} - \frac{2j(e^{j\psi_2} - e^{j\psi_3})}{\Omega}\cos\theta \right. \\ &\quad \left. + e^{j\psi_3}\cos^2\theta\right]. \end{aligned} \tag{35}$$

Note that $\sin\psi_i \approx \psi_i$ and $\cos\psi_i \gg \sin\psi_i$ for small microphone phase errors. Therefore, (35) can be further reduced to

$$\begin{aligned} \overline{E}_2^{(p)}(\theta) &\approx (1 - z_1 - z_2) + z_1(\cos\theta + (\psi_2 - \psi_3)/\Omega) \\ &\quad + z_2\left[2(\psi_2 - \psi_3)\cos\theta/\Omega + \cos^2\theta\right] \\ &\quad + jz_2(2\psi_2 - \psi_1 - \psi_3)/\Omega^2. \end{aligned} \tag{36}$$

Proposition 6: The mainlobe orientation of the second-order DMA is dependent of the microphone phase errors. Denote

$$T(\psi_i, \Omega) = (\psi_2 - \psi_3)/\Omega. \tag{37}$$

Then it follows that:

1) The mainlobe orientation is at 0° if the following conditions hold

1.1) For $T(\psi_i, \Omega) \geq 0$,

$$\begin{cases} 2\sqrt{z_2} - 2z_2 \leq z_1 \leq 1, & z_2 \in (0, 1/2) \quad (38a) \\ 2\sqrt{z_2} - 2z_2 \leq z_1 \leq 2\sqrt{2z_2} - 2z_2, & \\ \qquad\qquad z_2 \in [1/2, 12 - 8\sqrt{2}) \quad (38b) \\ 2\sqrt{z_2} - 2z_2 \leq z_1 < 2 - 3z_2/2, & z_2 \in [12 - 8\sqrt{2}, 1) \quad (38c) \\ 0 \leq z_1 < 2 - 3z_2/2, & z_2 \in [1, 4/3) \quad (38d) \end{cases}$$

1.2) For $\frac{3-\sqrt{2}-\sqrt{6-2\sqrt{2}}}{2} \leq T(\psi_i, \Omega) < 0$,

$$\begin{cases} 2\sqrt{z_2} - 2z_2 \leq z_1 \leq 1/(1 - T(\psi_i, \Omega)), \\ \qquad\qquad z_2 \in \left(0, \frac{1}{2(1-T(\psi_i,\Omega))^2}\right) \quad (39a) \\ 2\sqrt{z_2} - 2z_2 \leq z_1 \leq 2\sqrt{2z_2} - 2z_2(1 - T(\psi_i, \Omega)), \\ \quad z_2 \in \left[\frac{1}{2(1-T(\psi_i,\Omega))^2}, \right. \\ \qquad \left. \frac{12+16T(\psi_i,\Omega)-8\sqrt{2+8T(\psi_i,\Omega)}}{(1-4T(\psi_i,\Omega))^2}\right) \quad (39b) \\ 2\sqrt{z_2} - 2z_2 \leq z_1 < 2 - 3z_2/2, \\ \quad z_2 \in \left[\frac{12+16T(\psi_i,\Omega)-8\sqrt{2+8T(\psi_i,\Omega)}}{(1-4T(\psi_i,\Omega))^2}, \right. \\ \qquad \left. \frac{1}{(1-T(\psi_i,\Omega))^2}\right) \quad (39c) \\ -2z_2T(\psi_i, \Omega) \leq z_1 < 2 - 3z_2/2, \\ \qquad z_2 \in \left[\frac{1}{(1-T(\psi_i,\Omega))^2}, \frac{4}{3-4T(\psi_i,\Omega)}\right) \quad (39d) \end{cases}$$

1.3) For $\frac{1-\sqrt{3}}{4} \leq T(\psi_i, \Omega) < \frac{3-\sqrt{2}-\sqrt{6-2\sqrt{2}}}{2}$,

$$\begin{cases} 2\sqrt{z_2} - 2z_2 \leq z_1 \leq 1/(1 - T(\psi_i, \Omega)), \\ \qquad\qquad z_2 \in \left(0, \frac{1}{2(1-T(\psi_i,\Omega))^2}\right) \quad (40a) \\ 2\sqrt{z_2} - 2z_2 \leq z_1 \leq 2\sqrt{2z_2} - 2z_2(1 - T(\psi_i, \Omega)), \\ \qquad z_2 \in \left[\frac{1}{2(1-T(\psi_i,\Omega))^2}, \frac{1}{(1-T(\psi_i,\Omega))^2}\right) \quad (40b) \\ -2z_2T(\psi_i, \Omega) \leq z_1 < 2\sqrt{2z_2} - 2z_2(1 - T(\psi_i, \Omega)), \\ \quad z_2 \in \left[\frac{1}{(1-T(\psi_i,\Omega))^2}, \right. \\ \qquad \left. \frac{12+16T(\psi_i,\Omega)-8\sqrt{2+8T(\psi_i,\Omega)}}{(1-4T(\psi_i,\Omega))^2}\right) \quad (40c) \\ -2z_2T(\psi_i, \Omega) \leq z_1 < 2 - 3z_2/2, \\ \quad z_2 \in \left[\frac{12+16T(\psi_i,\Omega)-8\sqrt{2+8T(\psi_i,\Omega)}}{(1-4T(\psi_i,\Omega))^2}, \frac{4}{3-4T(\psi_i,\Omega)}\right) \quad (40d) \end{cases}$$

1.4) For $-\frac{\sqrt{2}}{2} \leq T(\psi_i, \Omega) < \frac{1-\sqrt{3}}{4}$,

$$\begin{cases} 2\sqrt{z_2} - 2z_2 \leq z_1 \leq 1/(1 - T(\psi_i, \Omega)), \\ \qquad\qquad z_2 \in \left(0, \frac{1}{2(1-T(\psi_i,\Omega))^2}\right) \quad (41a) \\ 2\sqrt{z_2} - 2z_2 \leq z_1 \leq 2\sqrt{2z_2} - 2z_2(1 - T(\psi_i, \Omega)), \\ \qquad z_2 \in \left[\frac{1}{2(1-T(\psi_i,\Omega))^2}, \frac{1}{(1-T(\psi_i,\Omega))^2}\right) \quad (41b) \\ -2z_2T(\psi_i, \Omega) \leq z_1 < 2\sqrt{2z_2} - 2z_2(1 - T(\psi_i, \Omega)), \\ \qquad z_2 \in \left[\frac{1}{(1-T(\psi_i,\Omega))^2}, \frac{2}{(1-2T(\psi_i,\Omega))^2}\right) \quad (41c) \end{cases}$$

1.5) For $-\sqrt{2} \leq T(\psi_i, \Omega) < -\frac{\sqrt{2}}{2}$,

$$\begin{cases} 2\sqrt{z_2} - 2z_2 \leq z_1 \leq 1/(1 - T(\psi_i, \Omega)), \\ \qquad\qquad z_2 \in \left(0, \frac{1}{2(1-T(\psi_i,\Omega))^2}\right) \quad (42a) \\ 2\sqrt{z_2} - 2z_2 \leq z_1 \leq 2\sqrt{2z_2} - 2z_2(1 - T(\psi_i, \Omega)), \\ \qquad z_2 \in \left[\frac{1}{2(1-T(\psi_i,\Omega))^2}, \frac{3-2\sqrt{2}}{T^2(\psi_i,\Omega)}\right) \quad (42b) \end{cases}$$

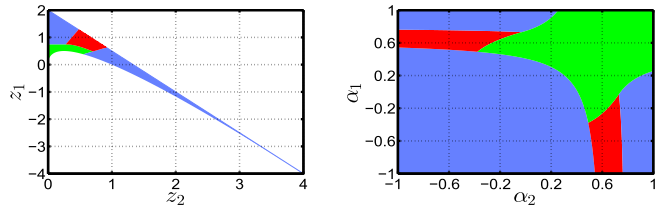

Fig. 13. (Color online) Mainlobe orientation of the second-order DMA with microphone phase errors versus (a) z_1 and z_2, and (b) α_1 and α_2, where $\psi_1 = -2.58°$, $\psi_2 = -0.86°$, $\psi_3 = 0.86°$, and $\Omega = \pi/36$ rad. The green, blue, and red areas correspond to the cases with mainlobe orientation of $0°$, $180°$, and $180° \pm \arccos(\frac{z_1}{2z_2} + T(\psi_i, \Omega))$ with $T(\psi_i, \Omega) = (\psi_2 - \psi_3)/\Omega$, respectively.

1.6) For $T(\psi_i, \Omega) < -\sqrt{2}$,

$$2\sqrt{z_2} - 2z_2 \le z_1 \le 1/(1 - T(\psi_i, \Omega)),$$

$$z_2 \in \left(0, \frac{\sqrt{2T(\psi_i,\Omega) - 2T^3(\psi_i,\Omega) + T^4(\psi_i,\Omega) - 1}}{2(1 - T(\psi_i,\Omega))^2} + \frac{-T(\psi_i,\Omega) + T^2(\psi_i,\Omega)}{2(1 - T(\psi_i,\Omega))^2}\right] \tag{43}$$

2) If (38)–(43) do not hold, then the mainlobe orientation is around $180° \pm \arccos(\frac{z_1}{2z_2} + T(\psi_i, \Omega))$ when $\frac{z_1}{2z_2} + T(\psi_i, \Omega) \in (-1, 1)$ and

$$z_1 \ge 2\sqrt{2z_2[1 + 4z_2(1 - T(\psi_i, \Omega))]} - 2z_2(3 - T(\psi_i, \Omega)),$$

or the mainlobe is oriented reversely to $180°$ when not.

Regarding the effects of microphone phase errors on the second-order DMA, we have the following remarks.

Remark 7: In contrast to the first-order DMA, the mainlobe of the second-order DMA with microphone phase errors is no longer always oriented toward the endfire directions. The possible mainlobe orientations of the second-order DMA include not only the endfire directions $0°$ and $180°$, but also the off-endfire directions $180° \pm \arccos(\frac{z_1}{2z_2} + (\psi_2 - \psi_3)/\Omega)$. The mainlobe orientation of the second-order DMA at the off-endfire directions depends on, in addition to the design parameters, the microphone phase errors and frequency, which is unlike the effect of microphone gain errors. With microphone gain errors, the mainlobe orientation of the second-order DMA at the off-endfire directions is only dependent on the design parameters. Specifically, the mainlobe orientation is independent on the phase error of the first microphone and only dependent on those of the second and third microphones. In addition, similar to the effect of microphone gain errors, the effect of microphone phase errors is also more significant in lower frequencies or for smaller array sizes.

Remark 8: Similar to the effect of microphone gain errors, the second-order DMA will be oriented toward the desired direction accurately without noticeable bias provided that the design parameters are appropriately set. To summarize, we can conclude that the first- and second-order DMAs with microphone mismatches will accurately be oriented toward $0°$ without noticeable errors when the mainlobe orientation is around the desired direction.

Next we demonstrate some numerical examples to justify the findings. Suppose the microphone phase errors $\psi_1 = -2.58°$, $\psi_2 = -0.86°$, $\psi_3 = 0.86°$, and $\Omega = \pi/36$ rad. Fig. 13(a) shows,

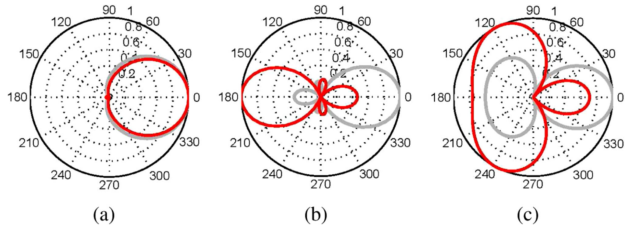

Fig. 14. Beampatterns of the second-order DMA with microphone phase errors (in red lines) for (a) $\alpha_1 = 0.5000$, $\alpha_2 = 0.5000$ (second-order cardioid); (b) $\alpha_1 = 0.4082$, $\alpha_2 = -0.4082$ (second-order hypercardioid response); and (c) $\alpha_1 = 0.6568$, $\alpha_2 = -0.4568$, where $\Omega = \pi/36$, rad. $\psi_1 = -2.58°$, $\psi_2 = -0.86°$ and $\psi_3 = 0.86°$. For comparison, the beampatterns without phase errors are also shown (in gray lines). The mainlobe orientations with microphone phase errors for (a), (b), and (c) are at $0°$, $180°$, and $180° \pm 62.86°$, respectively.

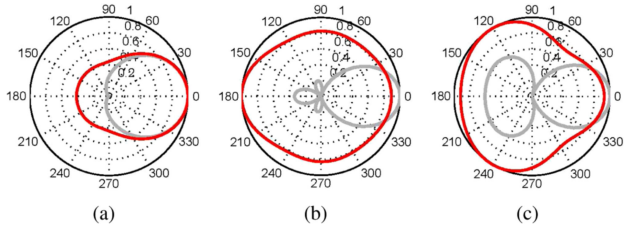

Fig. 15. Beampatterns of the second-order DMA with microphone phase errors (in red lines) for (a) $\alpha_1 = 0.5000$, $\alpha_2 = 0.5000$ (second-order cardioid); (b) $\alpha_1 = 0.4082$, $\alpha_2 = -0.4082$ (second-order hypercardioid response); and (c) $\alpha_1 = 0.6568$, $\alpha_2 = -0.4568$, where $\Omega = \pi/36$ rad., $\psi_1 = -2.01°$, $\psi_2 = -0.86°$ and $\psi_3 = 0.86°$. For comparison, the beampatterns without phase errors are also shown (in gray lines). The mainlobe orientations with microphone phase errors for (a), (b), and (c) are at $0°$, $180°$, and $180° \pm 62.86°$, respectively.

according to Proposition 6, the mainlobe orientation of the second-order DMA versus z_1 and z_2, where the green, blue, and red areas correspond to the cases with mainlobe orientation of $0°$, $180°$, and $180° \pm \arccos(\frac{z_1}{2z_2} + T(\psi_i, \Omega))$, respectively. By (10) and (11), we can obtain the corresponding mainlobe orientation of the second-order DMA as a function of the design parameters α_1 and α_2, shown in Fig. 13(b).

With the specified microphone phase errors, Figs. 14(a), 14(b), and 14(c) plot the beampatterns of three second-order DMAs with $\alpha_1 = 0.5000$, $\alpha_2 = 0.5000$; $\alpha_1 = 0.4082$, $\alpha_2 = -0.4082$; and $\alpha_1 = 0.6568$, $\alpha_2 = -0.4568$, respectively. For comparison, the corresponding beampatterns without microphone phase errors are also shown in the figures. Note that the design parameters α_1 and α_2 for Figs. 14(a), 14(b), and 14(c) are located in the green, blue, and red areas in Fig. 13(b), respectively. By Proposition 6, it follows that the mainlobe orientations of the three second-order DMAs should be theoretically at $0°$, $180°$, and $180° \pm \arccos(\frac{z_1}{2z_2} + T(\psi_i, \Omega)) = 180° \pm 62.86°$, respectively. From Fig. 14 we can see that the theoretically predicted mainlobe orientations are consistent with those in the simulation results. Particularly, for the second-order DMA with cardioid reponse in Fig. 14(a), its mainlobe is oriented around the desired direction, and as discussed above, there is indeed no noticeable orientation error.

To see the impact of the phase error of the first microphone, i.e., ψ_1, here we repeat the examples in Fig. 14 with a different value of ψ_1 and the remaining settings unchanged. The corresponding simulation results are shown in Fig. 15. Comparing with Fig. 14, we can see that the mainlobe orientations of the second-order DMAs in Fig. 15 are same as those in Fig. 14. This

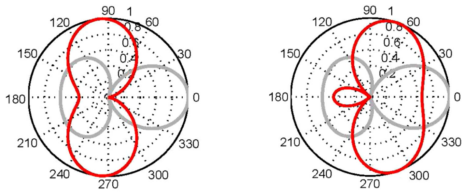

(a) (b)

Fig. 16. Beampatterns of the second-order DMA ($\alpha_1 = 0.6568$, $\alpha_2 = -0.4568$) with microphone phase errors (in red lines) for (a) $\Omega = \pi/72$ rad., $\psi_1 = -2.58°$, $\psi_2 = -0.86°$, $\psi_3 = 0.86°$; and (b) $\Omega = \pi/36$ rad., $\psi_1 = -8.59°$, $\psi_2 = -2.86°$, $\psi_3 = 2.86°$. For comparison, the beampattern without microphone phase errors is also shown (in gray lines), the mainlobe orientations with microphone phase errors for (a), (b) are at $180° \pm 83.54°$, $180° \pm 110.24°$, respectively.

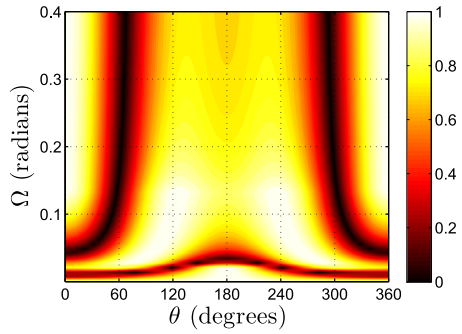

Fig. 17. Beampattern of the second-order DMA ($\alpha_1 = 0.6568$, $\alpha_2 = -0.4568$) with microphone phase errors as a function of Ω and θ, where $\psi_1 = -2.58°$, $\psi_2 = -0.86°$ and $\psi_3 = 0.86°$.

confirms our finding that the mainlobe orientation is independent on the phase error of microphone 1.

Figs. 16(a) and 16(b) show the beampatterns of the second-order DMA with $\alpha_1 = 0.6568$, $\alpha_2 = -0.4568$ (i.e., $z_1 = 0.8$, $z_2 = 0.5$) under different frequencies and microphone phase errors. For Fig. 16(a), we set $\Omega = \pi/72$ rad., $\psi_1 = -2.58°$, $\psi_2 = -0.86°$, $\psi_3 = 0.86°$. While for Fig. 16(b), we choose $\Omega = \pi/36$ rad., $\psi_1 = -8.59°$, $\psi_2 = -2.86°$, $\psi_3 = 2.86°$. In the two cases, the mainlobe orientations of the second-order DMA are both along the off-endfire directions. According to Proposition 6, we can deduce that the mainlobe orientations for Figs. 16(a) and 16(b) should be respectively at $180° \pm 83.54°$, $180° \pm 110.24°$, which are consistent with the simulation results. As revealed above, the off-endfire mainlobe orientation of the second-order DMA with microphone phase mismatches varies with frequency and microphone phase errors. This is unlike the effect of microphone gain errors, under which the off-endfire mainlobe orientation is fixed and independent on frequency and microphone gain errors.

Fig. 17 shows the beampattern of the second-order DMA with microphone phase errors as a function of Ω and θ, where the simulation conditions follow those in Fig. 16(a). From Fig. 17 we can see that, the mainlobe is correctly oriented toward the desired direction $0°$ at higher values of Ω, and with Ω decreasing the mainlobe is first wrongly oriented to the off-endfire directions and then to the reverse direction $180°$. This simulation result indicates that the effect of microphone phase errors becomes more prominent for smaller value of Ω, i.e., for lower frequencies or smaller array sizes, similar to the effect of microphone gain errors.

TABLE II
MICROPHONE GAIN-ERROR TOLERANCES FOR THE SECOND-ORDER DMAS WITH FREQUENCY BAND [200, 3700] HZ

DMA type	$d = 1$ cm	$d = 2$ cm
second-order cardioid	$\Delta_\epsilon \leq -64.4370$ dB	$\Delta_\epsilon \leq -51.3727$ dB
second-order supercardioid	$\Delta_\epsilon \leq -70.4576$ dB	$\Delta_\epsilon \leq -57.0774$ dB
second-order hypercardioid	$\Delta_\epsilon \leq -80.0000$ dB	$\Delta_\epsilon \leq -70.4576$ dB

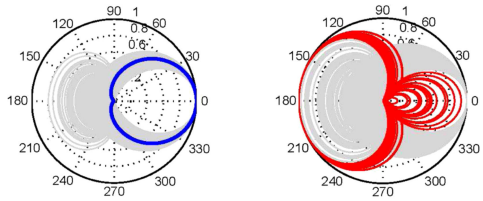

(a) (b)

Fig. 18. Beampatterns of the second-order cardioid DMA with varying microphone gain errors, where $d = 0.01$ m and $f \in [200, 3700]$ Hz. (a) $|\eta_i| \leq 0.0052$ dB; (b) $|\eta_i| \leq 0.0148$ dB, where the beampatterns with abnormal orientation are highlighted in red lines, and the ideal beampattern is also shown in blue line.

VI. MICROPHONE MISMATCH TOLERANCE ANALYSIS FOR CORRECT MAINLOBE ORIENTATION OF SECOND-ORDER DMA

In order to offer a useful guidance for practical design, in this section we perform an analysis on tolerance of microphone mismatches to ensure correct mainlobe orientation of the second-order DMA.

A. Microphone Gain-Error Tolerance Analysis

Proposition 7: Given the design specification of a second-order DMA, i.e., the array size d, the working frequency band $[f_l, f_h]$ and the design parameters α_1 and α_2, to guarantee the mainlobe orientation is always at $0°$, the tolerance of microphone gain errors Δ_ϵ should satisfy

$$\Delta_\epsilon \leq \frac{c^2 + 2\pi^2 f_l^2 d^2 \kappa - c\sqrt{c^2 + 8\pi^2 f_l^2 d^2 \kappa}}{2(c^2 - \pi^2 f_l^2 d^2 \kappa)} \tag{44}$$

where

$$\kappa = \begin{cases} \dfrac{(z_1 + 2z_2)^2 - 8z_2}{8z_2^2}, & \dfrac{z_1}{2z_2} \in (-1, 1) \\ \dfrac{z_1 - 1}{z_2}, & \text{otherwise,} \end{cases} \tag{45}$$

with z_1 and z_2 linked to α_1 and α_2 via (10) and (11).

For the speech communication applications with frequency band [200, 3700] Hz, the tolerances of microphone gain errors for the three typical second-order DMAs can be derived by Proposition 7, as shown in Table II. To guarantee correct mainlobe orientation, microphone gain errors (i.e., $|\eta_i - 1|$) should be less than the tolerance given in the table. Note also that the given tolerances of microphone gain errors are smaller than the gain errors of typical MEMS microphones, particularly at low frequency (c.f. Fig. 11 in [35]).

Several numerical examples are illustrated herein to evaluate the finding. Figs. 18–20 show the beampatterns of the three second-order DMAs, i.e., cardioid, supercardioid and hypercardioid, with an array size of 0.01 m and varying microphone gain errors. For each figure, we have performed 200 trials at each of the five distinct frequencies uniformly spaced in the frequency band of [200, 3700] Hz, i.e., 1000 trials in total. We can see from

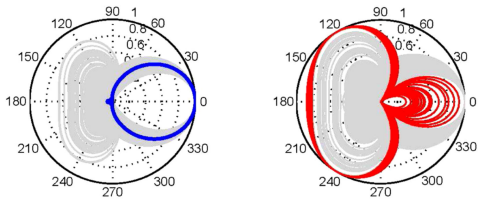

Fig. 19. Beampatterns of the second-order supercardioid DMA with varying microphone gain errors, where $d = 0.01$ m and $f \in [200, 3700]$ Hz. (a) $|\eta_i| \leq 0.0026$ dB; (b) $|\eta_i| \leq 0.0061$ dB, where the beampatterns with abnormal orientation are highlighted in red lines, and the ideal beampattern is also shown in blue line.

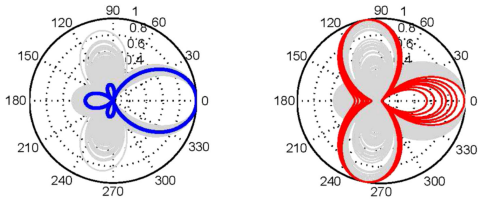

Fig. 20. Beampatterns of the second-order hypercardioid DMA with varying microphone gain errors, where $d = 0.01$ m and $f \in [200, 3700]$ Hz. (a) $|\eta_i| \leq 0.0008$ dB; (b) $|\eta_i| \leq 0.0026$ dB, where the beampatterns with abnormal orientation are highlighted in red lines, and the ideal beampattern is also shown in blue line.

Figs. 18(a), 19(a) and 20(a) that, under the condition that the microphone gain errors are all less than the maximum tolerances, all the mainlobes are correctly oriented toward 0°. However, when the maximum tolerances of microphone gain errors are violated, it may lead to abnormal mainlobe orientation as shown in Figs. 18(b), 19(b) and 20(b), where the beampatterns with abnormal mainlobe orientation have been highlighted in red.

B. Microphone Phase-Error Tolerance Analysis

Proposition 8: Given the design specification of a second-order DMA, i.e., the array size d, the working frequency band $[f_l, f_h]$ and the design parameters α_1 and α_2, to guarantee the mainlobe orientation is always at 0°, the tolerance of microphone phase errors Δ_ψ should satisfy

$$\Delta_\psi \leq \begin{cases} \dfrac{\pi f_l d(1-z_1)}{cz_1}, & z_1^2 - 2z_2 + 4z_1 z_2 \leq 0 \text{ or } z_1 \geq \sqrt{2z_2} \\ \min\left\{ \dfrac{\pi f_l d(\sqrt{8z_2} - 2z_2 - z_1)}{2cz_2}, \dfrac{\pi f_l d z_1}{2cz_2} \right\}, & \\ \qquad \sqrt{2z_2} - 2z_2 < z_1 < \sqrt{2z_2} \end{cases} \tag{46}$$

with z_1 and z_2 linked to α_1 and α_2 via (10) and (11).

For the speech communication applications with frequency band [200, 3700] Hz, Table III shows the microphone phase-error tolerances for the three typical second-order DMAs according to Proposition 8.

In the following, we present several numerical examples to verify the finding. Figs. 21–23 show the beampatterns of the three typical second-order DMAs with an array size of 0.01 m and varying microphone phase errors. For Figs. 21(a), 22(a) and 23(a), we performed 500 trials at each of the five distinct frequencies uniformly spaced in the frequency band of [200, 3700] Hz, i.e., totally 2500 trials for each figure. While for Figs. 21(b), 22(b) and 23(b), 1000 trials are carried out at each of the five frequencies, i.e., totally 5000 trials for each figure. From Figs. 21(a), 22(a) and 23(a) we can see that, since the microphone phase errors are all within the maximum tolerances, all the beampatterns can be correctly oriented toward 0°. By contrast, when the microphone phase-error tolerances cannot be satisfied, it indeed results in abnormal mainlobe orientation as shown in Figs. 21(b), 22(b) and 23(b), where the beampatterns with abnormal mainlobe orientation are highlighted in red.

TABLE III
MICROPHONE PHASE-ERROR TOLERANCES FOR THE SECOND-ORDER DMAS WITH FREQUENCY BAND [200, 3700] HZ

DMA type	$d = 1$ cm	$d = 2$ cm
second-order cardioid	$\Delta_\psi \leq 0.8772^\circ$	$\Delta_\psi \leq 1.7543^\circ$
second-order supercardioid	$\Delta_\psi \leq 0.5603^\circ$	$\Delta_\psi \leq 1.1206^\circ$
second-order hypercardioid	$\Delta_\psi \leq 0.2118^\circ$	$\Delta_\psi \leq 0.4235^\circ$

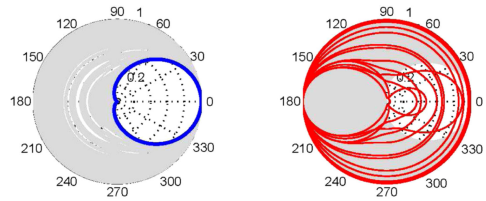

Fig. 21. Beampatterns of the second-order cardioid DMA with varying microphone phase errors, where $d = 0.01$ m and $f \in [200, 3700]$ Hz. (a) $|\psi_i| \leq 0.8772^\circ$; (b) $|\psi_i| \leq 4.3149^\circ$, where the beampatterns with abnormal orientation are highlighted in red lines, and the ideal beampattern is also shown in blue line.

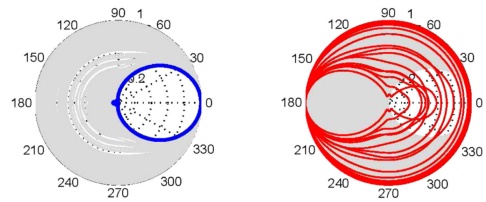

Fig. 22. Beampatterns of the second-order supercardioid DMA with varying microphone phase errors, where $d = 0.01$ m and $f \in [200, 3700]$ Hz. (a) $|\psi_i| \leq 0.5603^\circ$; (b) $|\psi_i| \leq 2.8521^\circ$, where the beampatterns with abnormal orientation are highlighted in red lines, and the ideal beampattern is also shown in blue line.

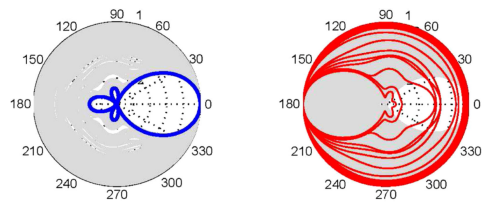

Fig. 23. Beampatterns of the second-order hypercardioid DMA with varying microphone phase errors, where $d = 0.01$ m and $f \in [200, 3700]$ Hz. (a) $|\psi_i| \leq 0.2118^\circ$; (b) $|\psi_i| \leq 2.1400^\circ$, where the beampatterns with abnormal orientation are highlighted in red lines, and the ideal beampattern is also shown in blue line.

C. Simultaneous Effect of Microphone Gain and Phase Errors

As we have discussed, unlike the first-order DMAs, both microphone gain and phase errors may pose detrimental effect on

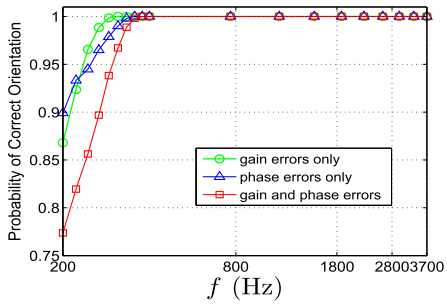

Fig. 24. Comparison of the probabilities of correct mainlobe orientation for the second-order hypercardioid DMA with microphone gain errors only ($|\eta_i| \leq 0.0035$ dB), with microphone phase errors only ($|\psi_i| \leq 0.4297^\circ$), and with microphone gain and phase errors ($|\eta_i| \leq 0.0035$ dB, $|\psi_i| \leq 0.4297^\circ$), where $d = 0.01$ m. For each evaluated frequency, 1×10^4 trials are conducted.

mainlobe orientation of the second-order DMAs. In the above, we have derived the maximum tolerances of microphone gain and phase errors to ensure correct mainlobe orientation of the second-order DMAs under a design specification, i.e., (44) and (46). We would like to point out that, as expected, (44) and (46) are necessary conditions to ensure correct mainlobe orientation of the second-order DMAs when microphone gain and phase errors are present simultaneously. To justify the above discussion, Fig. 24 compares the probabilities of correct mainlobe orientation of the second-order hypercardioid DMA over the frequency band [200, 3700] Hz with $d = 0.01$ m for the three scenarios: i) with microphone gain errors only ($|\eta_i| \leq 0.0035$ dB); ii) with microphone phase errors only ($|\psi_i| \leq 0.4297^\circ$); and iii) with microphone gain and phase errors simultaneously ($|\eta_i| \leq 0.0035$ dB, $|\psi_i| \leq 0.4297^\circ$). Herein, for each evaluated frequency, 1×10^4 trials have been conducted. Note that the microphone gain and phase errors both are greater than their maximum tolerances, i.e., -80 dB and 0.2118° as given in Tables II and III. Moreover, as discussed above, the effect of microphone mismatches is more significant in lower frequencies. Consequently, we can see from Fig. 24 that, for the two scenarios with microphone gain errors only or with microphone phase errors only, the mainlobe misorientation problem occurs at lower frequencies. More to our interest, as shown in Fig. 24, compared with either of the two scenarios, the mainlobe misorientation problem for the scenario with microphone gain and phase errors simultaneously is deteriorated more significantly. This implies that, to ensure the correct mainlobe orientation with microphone gain and phase errors simultaneously, we at least need to ensure the correct mainlobe orientation both with microphone gain errors only and with microphone phase errors only, i.e., (44) and (46) are necessary conditions to be satisfied.

VII. Conclusions

In this paper, we have studied the effects of microphone mismatches on mainlobe orientation of the first- and second-order DMAs. It is shown that the mainlobe orientation of first-order DMAs is independent on microphone gain errors and only dependent on microphone phase errors. For second-order DMAs, however, both microphone gain and phase errors may lead to serious mainlobe misorientation problem. To provide a useful guidance for practical design, microphone mismatch tolerance analysis has also been carried out to guarantee correct mainlobe orientation of the two types of DMAs.

Appendix A
Proof of Proposition 1

We show first that (14) should be satisfied to guarantee the mainlobe is oriented toward 0°. To this end, taking the derivative of $|\overline{E}_2(\theta)|^2$ with respect to θ, we have

$$\begin{aligned}\frac{\mathrm{d}\{|\overline{E}_2(\theta)|^2\}}{\mathrm{d}\theta} &= -2((1-z_1-z_2)+z_1\cos\theta+z_2\cos^2\theta)\\ &\quad\times(z_1+2z_2\cos\theta)\sin\theta\\ &= -2\overline{E}_2(\theta)(z_1+2z_2\cos\theta)\sin\theta. \end{aligned} \tag{47}$$

The extrema of $|\overline{E}_2(\theta)|^2$ should satisfy $\overline{E}_2(\theta)=0$ or $(z_1+2z_2\cos\theta)\sin\theta=0$. Since $\overline{E}_2(\theta)=0$ corresponds to minima, we only need to consider the remaining extrema, i.e., $\theta = 180^\circ \pm \arccos(\frac{z_1}{2z_2})$, 0° and 180°, which correspond to $(z_1+2z_2\cos\theta)\sin\theta=0$. Then we have the following two cases to consider in terms of $\frac{z_1}{2z_2}$:

1) $\frac{z_1}{2z_2} \in (-1,1)$. To guarantee the mainlobe orientation is at 0°, the array response at 0° should be no less than those at other three maxima. Accordingly, it follows that
   - for $|\overline{E}_2(0^\circ)|^2 \geq |\overline{E}_2(180^\circ)|^2$, we obtain $0 \leq z_1 \leq 1$.
   - for $|\overline{E}_2(0^\circ)|^2 \geq |\overline{E}_2(180^\circ \pm \arccos(\frac{z_1}{2z_2}))|^2$, we have $[1-z_1-z_2-\frac{z_1^2}{4z_2}]^2 \leq 1$. It implies that $-2\sqrt{2z_2}-2z_2 \leq z_1 \leq 2\sqrt{2z_2}-2z_2$ with $z_2>0$.

   Summarizing and further noticing (13), we have

$$\begin{cases} 2\sqrt{z_2}-2z_2 \leq z_1 < 2z_2, & z_2 \in \left(\frac{1}{4},\frac{1}{2}\right) \quad (48a)\\ 2\sqrt{z_2}-2z_2 \leq z_1 \leq 2\sqrt{2z_2}-2z_2, & z_2 \in \left[\frac{1}{2}, 12-8\sqrt{2}\right) \quad (48b)\\ 2\sqrt{z_2}-2z_2 \leq z_1 < 2-3z_2/2, & z_2 \in [12-8\sqrt{2},1) \quad (48c)\\ 0 \leq z_1 < 2-3z_2/2, & z_2 \in \left[1,\frac{4}{3}\right) \quad (48d) \end{cases}$$

2) $\frac{z_1}{2z_2} \notin (-1,1)$. In this case, we can derive that there are two extrema at $\theta = 0^\circ$ and 180°. By $|\overline{E}_2(0^\circ)|^2 \geq |\overline{E}_2(180^\circ)|^2$, we get $(1-2z_1)^2 \leq 1$, which implies $0 \leq z_1 \leq 1$. Further note (13), we obtain

$$\begin{cases} 2\sqrt{z_2}-2z_2 \leq z_1 \leq 1, & z_2 \in \left(0,\frac{1}{4}\right) \quad (49a)\\ 2z_2 \leq z_1 \leq 1, & z_2 \in \left[\frac{1}{4},\frac{1}{2}\right] \quad (49b) \end{cases}$$

Combing (48) and (49) yields (14). This means that (14) should hold to keep the mainlobe orientation at 0°.

Next we consider the scenario when (14) does not hold. In this scenario, the mainlobe orientation is either at $180^\circ \pm \arccos(z_1/(2z_2))$ or 180°, instead of the desired direction 0°. As analyzed above, for $\frac{z_1}{2z_2} \in (-1,1)$ there exist four extrema. If $z_1 \geq 2\sqrt{2z_2+8z_2^2}-6z_2$, then we have

$$|\overline{E}_2(180^\circ \pm \arccos(z_1/(2z_2)))|^2 \geq |\overline{E}_2(0^\circ)|^2 \tag{50}$$

$$|\overline{E}_2(180^\circ \pm \arccos(z_1/(2z_2)))|^2 \geq |\overline{E}_2(180^\circ)|^2. \tag{51}$$

This implies that the mainlobe is oriented toward $180^\circ \pm \arccos(z_1/(2z_2))$. Otherwise, i.e., if $z_1 < 2\sqrt{2z_2 + 8z_2^2} - 6z_2$, it follows that

$$|\overline{E}_2(180^\circ)|^2 \geq |\overline{E}_2(0^\circ)|^2 \tag{52}$$

$$|\overline{E}_2(180^\circ)|^2 \geq |\overline{E}_2(180^\circ \pm \arccos(z_1/(2z_2)))|^2. \tag{53}$$

It implies that the mainlobe is oriented toward 180°. For $\frac{z_1}{2z_2} \notin (-1, 1)$, there are two local maxima at $\theta = 0^\circ$ and 180°. In this case, we have $|\overline{E}_2(180^\circ)|^2 \geq |\overline{E}_2(0^\circ)|^2$, i.e., the mainlobe is also oriented toward 180°.

Appendix B
Proof of Proposition 2

Taking the derivative of $|\overline{E}_1^{(g)}(\theta)|^2$ with respect to θ yields

$$\begin{aligned} \mathrm{d}\{|\overline{E}_1^{(g)}(\theta)|^2\}/\mathrm{d}\theta &= 2\eta_2^2[\alpha + (1-\alpha)\cos\theta](\alpha - 1)\sin\theta \\ &= 2\eta_2 \Re\{\overline{E}_1^{(g)}(\theta)\}(\alpha - 1)\sin\theta. \end{aligned} \tag{54}$$

where $\Re\{\cdot\}$ denotes the real part.

By (54), the extrema of $|\overline{E}_1^{(g)}(\theta)|^2$ should satisfy $\Re\{\overline{E}_1^{(g)}(\theta)\} = 0$ or $\sin\theta = 0$. Note that if $\Re\{\overline{E}_1^{(g)}(\theta)\}|_{\theta=\theta_0} = 0$, then for arbitrary $\theta \in [0^\circ, 360^\circ)$ we have $(|\overline{E}_1^{(g)}(\theta)|^2)_{\theta=\theta_0} \leq |\overline{E}_1^{(g)}(\theta)|^2$, i.e., $\Re\{\overline{E}_1^{(g)}(\theta)\} = 0$ is corresponding to minima. Therefore, it suffices to consider the extrema $\theta = 0^\circ$ and 180°. Further note that $|\overline{E}_1^{(g)}(0^\circ)|^2 - |\overline{E}_1^{(g)}(180^\circ)|^2 = 4\eta_2^2\alpha(1-\alpha) \geq 0$. Therefore, the mainlobe orientation of the first-order DMAs is always at the desired direction 0°, which is independent of microphone gain errors.

Appendix C
Proof of Proposition 3

By (22), we have

$$\begin{aligned} \frac{\mathrm{d}\{|\overline{E}_1^{(p)}(\theta)|^2\}}{\mathrm{d}\theta} &= 2\left[\alpha + (1-\alpha)\cos\theta + \frac{(1-\alpha)(\psi_1 - \psi_2)}{\Omega}\right] \\ &\quad \times (\alpha - 1)\sin\theta \\ &= 2\overline{E}_1^{(p)}(\theta)(\alpha - 1)\sin\theta. \end{aligned} \tag{55}$$

Accordingly, the extrema should satisfy either $\overline{E}_1^{(p)}(\theta) = 0$ or $\sin\theta = 0$. Evidently, $\overline{E}_1^{(p)}(\theta)$ implies minima, thus we only need to consider the extrema $\theta = 0^\circ$ and 180°.

To guarantee the mainlobe orientation is at $\theta = 0^\circ$, it suffices to ensure $|\overline{E}_1^{(p)}(0)|^2 \geq |\overline{E}_1^{(p)}(180^\circ)|^2$. By (18), this is equivalent to $(1-\alpha)[\alpha + (1-\alpha)(\psi_1 - \psi_2)/\Omega] \geq 0$. Note that $\alpha \in [0, 1)$. Therefore it further reduces to

$$\alpha + (1-\alpha)(\psi_1 - \psi_2)/\Omega \geq 0. \tag{56}$$

We have two cases to consider in terms of ψ_1 and ψ_2:

1) if $\psi_1 \geq \psi_2$, for an arbitrary $\alpha \in [0, 1)$, we can deduce that (56) holds.

2) Note that Ω is nonnegative. For $\psi_1 < \psi_2$, we have $\frac{\psi_1 - \psi_2}{\psi_1 - \psi_2 - \Omega} \in [0, 1)$. Then we can also deduce that (56) holds if $\psi_1 < \psi_2$ with $\frac{\psi_1 - \psi_2}{\psi_1 - \psi_2 - \Omega} \leq \alpha < 1$. Otherwise, i.e., when $\psi_1 < \psi_2$ with $0 \leq \alpha < \frac{\psi_1 - \psi_2}{\psi_1 - \psi_2 - \Omega}$, we obtain $|\overline{E}_1^{(p)}(0^\circ)|^2 < |\overline{E}_1^{(p)}(180^\circ)|^2$. It implies that the mainlobe orientation of the first-order DMAs is at 180°.

Appendix D
Proof of Proposition 4

Since $f \in [f_l, f_h]$, then we have $\Omega \in [\frac{2\pi d}{c} f_l, \frac{2\pi d}{c} f_h] \triangleq [\underline{\Omega}, \overline{\Omega}]$. To guarantee the mainlobe orientation of the first-order DMA is always at 0°, we have the following cases to consider:

1) $\psi_1 \geq \psi_2$. For an arbitrary $\alpha \in [0, 1)$, it follows from Proposition 3 that the mainlobe orientation is always at 0°.

2) $\psi_1 < \psi_2$. Denote $\chi_1 = \psi_1 - \psi_2$. Then α_T can be reformulated as $\alpha_T \triangleq \frac{\chi_1}{\chi_1 - \Omega}$. Taking the derivative of α_T with respect to χ_1 and Ω yields $\frac{\partial \alpha_T}{\partial \chi_1} = \frac{\chi_1}{(\chi_1 - \Omega)^2} < 0$ and $\frac{\partial \alpha_T}{\partial \Omega} = -\frac{\Omega}{(\chi_1 - \Omega)^2} < 0$, i.e., α_T is the decreasing function of χ_1 and Ω. Since $\psi_i \in [-\Delta_\psi, \Delta_\psi]$, we get $\alpha_T = \frac{\chi_1}{\chi_1 - \Omega} \in (0, \frac{2\Delta_\psi}{2\Delta_\psi + \underline{\Omega}}]$. According to Proposition 3, if the mainlobe orientation is at 0°, α_T should satisfy $\alpha_T \leq \alpha$, which means $\frac{2\Delta_\psi}{2\Delta_\psi + \underline{\Omega}} \leq \alpha$. Therefore, the tolerance of microphone phase errors should satisfy $\Delta_\psi \leq \frac{\pi f_l d \alpha}{c(1-\alpha)}$.

Appendix E
Proof of Proposition 5

Taking the derivative of $|\overline{E}_2^{(g)}(\theta)|^2$ with respect to θ, we get

$$\begin{aligned} \frac{\mathrm{d}\{|\overline{E}_2^{(g)}(\theta)|^2\}}{\mathrm{d}\theta} &= -2\Bigg\{[\eta_3^2(1 - z_1 - z_2) + z_1\eta_3^2\cos\theta \\ &\quad + z_2\eta_3\left(\frac{2\eta_2 - \eta_1 - \eta_3}{\Omega^2} + \eta_3\cos^2\theta\right)\Bigg] \\ &\quad + \frac{2z_2(\eta_2 - \eta_3)^2}{\Omega^2}\Bigg\}(z_1 + 2z_2\cos\theta)\sin\theta \\ &= -2\left[\eta_3\Re\{\overline{E}_2^{(g)}(\theta)\} + \frac{2z_2(\eta_2 - \eta_3)^2}{\Omega^2}\right] \\ &\quad \times (z_1 + 2z_2\cos\theta)\sin\theta. \end{aligned} \tag{57}$$

By (57), it follows that the extrema should satisfy either $\eta_3\Re\{\overline{E}_2^{(g)}(\theta)\} + \frac{2z_2(\eta_2 - \eta_3)^2}{\Omega^2} = 0$ or $(z_1 + 2z_2\cos\theta)\sin\theta = 0$.

Suppose that when $\theta = \theta_0$, it holds that $\eta_3\Re\{\overline{E}_2^{(g)}(\theta)\} + \frac{2z_2(\eta_2 - \eta_3)^2}{\Omega^2} = 0$. Then we have

$$\frac{\mathrm{d}^2\{|\overline{E}_2^{(g)}(\theta)|^2\}}{\mathrm{d}\theta^2}|_{\theta=\theta_0} = 2\eta_3^2(z_1 + 2z_2\cos\theta_0)^2\sin^2\theta_0 \geq 0. \tag{58}$$

Recall that $\frac{\mathrm{d}\{|\overline{E}_2^{(g)}(\theta)|^2\}}{\mathrm{d}\theta}|_{\theta=\theta_0} = 0$. If $\frac{\mathrm{d}^2\{|\overline{E}_2^{(g)}(\theta)|^2\}}{\mathrm{d}\theta^2}|_{\theta=\theta_0} > 0$, then we can conclude that $\theta = \theta_0$ is corresponding to a minimum. Otherwise, i.e., $\frac{\mathrm{d}^2\{|\overline{E}_2^{(g)}(\theta)|^2\}}{\mathrm{d}\theta^2}|_{\theta=\theta_0} = 0$, it implies $(z_1 + 2z_2\cos\theta)\sin\theta = 0$. To summarize, we only need to consider the extrema that satisfy $(z_1 + 2z_2\cos\theta)\sin\theta = 0$. We have the following two cases to consider in terms of $\frac{z_1}{2z_2}$:

1) $\frac{z_1}{2z_2} \in (-1, 1)$. In this case, there exist four extrema, i.e., $\theta = 180^\circ \pm \arccos(\frac{z_1}{2z_2})$, 0 and 180°, that satisfy $(z_1 + 2z_2\cos\theta)\sin\theta = 0$. To ensure the mainlobe orientation is at 0°, the following two conditions should hold. One condition is $|\overline{E}_2^{(g)}(0^\circ)|^2 \geq |\overline{E}_2^{(g)}(180^\circ)|^2$, i.e.,

$$\begin{aligned} &(\eta_3 + z_2(2\eta_2 - \eta_1 - \eta_3)/\Omega^2)^2 + (z_1 + 2z_2)^2(\eta_3 - \eta_2)^2/\Omega^2 \\ &\quad - \left[\eta_3(1 - 2z_1) + z_2(2\eta_2 - \eta_1 - \eta_3)/\Omega^2\right]^2 \\ &\quad - (z_1 - 2z_2)^2(\eta_3 - \eta_2)^2/\Omega^2 \geq 0. \end{aligned} \tag{59}$$

By (26), (59) can be reduced to

$$0 \le z_1 \le 1 + z_2 G(\eta_i, \Omega). \tag{60}$$

The other condition is $|\overline{E}_2^{(g)}(0^\circ)|^2 \ge |\overline{E}_2^{(g)}(180^\circ \pm \arccos(\frac{z_1}{2z_2}))|^2$, which implies that

$$\begin{aligned}&[\eta_3 + z_2(2\eta_2 - \eta_1 - \eta_3)/\Omega^2]^2 + (z_1 + 2z_2)^2(\eta_3 - \eta_2)^2/\Omega^2 \\ &\quad - [\eta_3(1 - z_1 - z_2 - z_1^2/(4z_2)) \\ &\quad + z_2(2\eta_2 - \eta_1 - \eta_3)/\Omega^2]^2 \ge 0.\end{aligned} \tag{61}$$

By (26), (61) can be simplified as

$$\begin{aligned}&-2\sqrt{2z_2 + 2z_2^2 G(\eta_i, \Omega))} \\ &-2z_2 \le z_1 \le 2\sqrt{2z_2 + 2z_2^2 G(\eta_i, \Omega))} - 2z_2.\end{aligned} \tag{62}$$

Note that in this case $G(\eta_i, \Omega) \ge -2$. With (13), (60) and (62), we further have

1.1) For $G(\eta_i, \Omega) \ge 0$,

$$\begin{cases} 2\sqrt{z_2} - 2z_2 \le z_1 < 2z_2, & z_2 \in \left[\frac{1}{4}, \frac{1}{2}\right) \quad (63a) \\ 2\sqrt{z_2} - 2z_2 \le z_1 \le 2\sqrt{2z_2} - 2z_2, & z_2 \in \left[\frac{1}{2}, 12 - 8\sqrt{2}\right) \quad (63b) \\ 2\sqrt{z_2} - 2z_2 \le z_1 < 2 - 3z_2/2, & z_2 \in [12 - 8\sqrt{2}, 1) \quad (63c) \\ 0 \le z_1 < 2 - 3z_2/2, & z_2 \in \left[1, \frac{4}{3}\right) \quad (63d) \end{cases}$$

1.2) For $-\frac{7}{32} \le G(\eta_i, \Omega) < 0$,

$$\begin{cases} 2\sqrt{z_2} - 2z_2 \le z_1 < 2z_2, \quad z_2 \in \left[\frac{1}{4}, \frac{1}{2 - G(\eta_i, \Omega)}\right) & (64a) \\ 2\sqrt{z_2} - 2z_2 \le z_1 \le 2\sqrt{2z_2 + 2z_2^2 G(\eta_i, \Omega)} - 2z_2, \\ \qquad z_2 \in \left[\frac{1}{2 - G(\eta_i, \Omega)}, \frac{12 - 8\sqrt{2 + 8G(\eta_i, \Omega)}}{1 - 32G(\eta_i, \Omega)}\right) & (64b) \\ 2\sqrt{z_2} - 2z_2 \le z_1 < 2 - 3z_2/2, \\ \qquad z_2 \in \left[\frac{12 - 8\sqrt{2 + 8G(\eta_i, \Omega)}}{1 - 32G(\eta_i, \Omega)}, 1\right) & (64c) \\ 0 \le z_1 < 2 - 3z_2/2, \quad z_2 \in \left[1, \frac{4}{3}\right) & (64d) \end{cases}$$

1.3) For $-\frac{1}{4} \le G(\eta_i, \Omega) < -\frac{7}{32}$,

$$\begin{cases} 2\sqrt{z_2} - 2z_2 \le z_1 < 2z_2, \quad z_2 \in \left[\frac{1}{4}, \frac{1}{2 - G(\eta_i, \Omega)}\right) & (65a) \\ 2\sqrt{z_2} - 2z_2 \le z_1 \le 2\sqrt{2z_2 + 2z_2^2 G(\eta_i, \Omega)} - 2z_2, \\ \qquad z_2 \in \left[\frac{1}{2 - G}, 1\right) & (65b) \\ 0 \le z_1 \le 2\sqrt{2z_2 + 2z_2^2 G(\eta_i, \Omega)} - 2z_2, \\ \qquad z_2 \in \left[1, \frac{12 - 8\sqrt{2 + 8G(\eta_i, \Omega)}}{1 - 32G(\eta_i, \Omega)}\right) & (65c) \\ 0 \le z_1 < 2 - 3z_2/2, \\ \qquad z_2 \in \left[\frac{12 - 8\sqrt{2 + 8G(\eta_i, \Omega)}}{1 - 32G(\eta_i, \Omega)}, \frac{4}{3}\right) & (65d) \end{cases}$$

1.4) For $-\frac{1}{2} \le G(\eta_i, \Omega) < -\frac{1}{4}$,

$$\begin{cases} 2\sqrt{z_2} - 2z_2 \le z_1 < 2z_2, \quad z_2 \in \left[\frac{1}{4}, \frac{1}{2 - G(\eta_i, \Omega)}\right) & (66a) \\ 2\sqrt{z_2} - 2z_2 \le z_1 \le 2\sqrt{2z_2 + 2z_2^2 G(\eta_i, \Omega)} - 2z_2, \\ \qquad z_2 \in \left[\frac{1}{2 - G(\eta_i, \Omega)}, 1\right) & (66b) \\ 0 \le z_1 \le 2\sqrt{2z_2 + 2z_2^2 G(\eta_i, \Omega)} - 2z_2, \\ \qquad z_2 \in \left[1, \frac{2}{1 - 2G(\eta_i, \Omega)}\right] & (66c) \end{cases}$$

1.5) For $-2 \le G(\eta_i, \Omega) < -\frac{1}{2}$,

$$\begin{cases} 2\sqrt{z_2} - 2z_2 \le z_1 < 2z_2, \quad z_2 \in \left[\frac{1}{4}, \frac{1}{2 - G(\eta_i, \Omega)}\right) & (67a) \\ 2\sqrt{z_2} - 2z_2 \le z_1 \le 2\sqrt{2z_2 + 2z_2^2 G(\eta_i, \Omega)} - 2z_2, \\ \qquad z_2 \in \left[\frac{1}{2 - G(\eta_i, \Omega)}, -\frac{1}{2G(\eta_i, \Omega)}\right] & (67b) \end{cases}$$

2) $\frac{z_1}{2z_2} \notin (-1, 1)$. In this case, there only exist two extrema, 0° and 180°, that satisfy $(z_1 + 2z_2 \cos\theta)\sin\theta = 0$. To guarantee the mainlobe orientation is at 0°, it suffices that $|\overline{E}_2^{(g)}(0^\circ)|^2 \ge |\overline{E}_2^{(g)}(180^\circ)|^2$, which means that

$$0 \le z_1 \le 1 + z_2 G(\eta_i, \Omega). \tag{68}$$

Combining (68) with (13), we have

2.1) For $G(\eta_i, \Omega) \ge 0$,

$$\begin{cases} 2\sqrt{z_2} - 2z_2 \le z_1 \le 1, & z_2 \in \left(0, \frac{1}{4}\right) \quad (69a) \\ 2z_2 \le z_1 \le 1, & z_2 \in \left[\frac{1}{4}, \frac{1}{2}\right] \quad (69b) \end{cases}$$

2.2) For $-2 \le G(\eta_i, \Omega) < 0$,

$$\begin{cases} 2\sqrt{z_2} - 2z_2 \le z_1 \le 1 + z_2 G(\eta_i, \Omega), & z_2 \in \left(0, \frac{1}{4}\right) \quad (70a) \\ 2z_2 \le z_1 \le 1 + z_2 G(\eta_i, \Omega), & z_2 \in \left[\frac{1}{4}, \frac{1}{2 - G(\eta_i, \Omega)}\right] \quad (70b) \end{cases}$$

2.3) For $G(\eta_i, \Omega) < -2$,

$$\begin{aligned}&2\sqrt{z_2} - 2z_2 \le z_1 \le 1 + z_2 G(\eta_i, \Omega), \\ &\qquad z_2 \in \left(0, \frac{-2\sqrt{-1 - G(\eta_i, \Omega)} - G(\eta_i, \Omega)}{(2 + G(\eta_i, \Omega))^2}\right]\end{aligned} \tag{71}$$

Finally, to simplify the results, we can merge (63) with (69), (64) with (70), (65) with (70), (66) with (70), and (67) with (70), which yield (27), (28), (29), (30) and (31), respectively. In addition, (71) leads directly to (32).

Next we consider the scenario when (27)–(32) does not hold. In this scenario, the mainlobe orientation is either at $180^\circ \pm \arccos(z_1/(2z_2))$ or 180°. For $\frac{z_1}{2z_2} \in (-1, 1)$ there exist four extrema. If $z_1 \ge 2\sqrt{2z_2[1 + (4 + G(\eta_i, \Omega))z_2]} - 6z_2$, then we get

$$|\overline{E}_2^{(g)}(180^\circ \pm \arccos(z_1/(2z_2)))|^2 \ge |\overline{E}_2^{(g)}(0^\circ)|^2 \tag{72}$$

$$|\overline{E}_2^{(g)}(180^\circ \pm \arccos(z_1/(2z_2)))|^2 \ge |\overline{E}_2^{(g)}(180^\circ)|^2. \tag{73}$$

It means that the mainlobe is oriented toward $180^\circ \pm \arccos(z_1/(2z_2))$. Otherwise, i.e., if

$$z_1 < 2\sqrt{2z_2[1+(4+G(\eta_i,\Omega))z_2]} - 6z_2,$$

we have

$$|\overline{E}_2^{(g)}(180^\circ)|^2 \geq |\overline{E}_2^{(g)}(0^\circ)|^2 \tag{74}$$

$$|\overline{E}_2^{(g)}(180^\circ)|^2 \geq |\overline{E}_2^{(g)}(180^\circ \pm \arccos(z_1/(2z_2)))|^2. \tag{75}$$

For $\frac{z_1}{2z_2} \notin (-1,1)$, there are two local maxima at $\theta = 0^\circ$ and 180°. In this case, we have $|\overline{E}_2^{(g)}(180^\circ)|^2 \geq |\overline{E}_2^{(g)}(0^\circ)|^2$, i.e., the mainlobe is also oriented toward 180°.

Appendix F
Proof of Proposition 6

With (36), we obtain

$$\begin{aligned}\frac{\mathrm{d}\{|\overline{E}_2^{(p)}(\theta)|^2\}}{\mathrm{d}\theta} =& -2\{[(1-z_1-z_2)+z_1(\cos\theta+T(\psi_i,\Omega)) \\ &+ z_2(2T\cos\theta+\cos^2\theta)\} \\ &\times [z_1+2z_2(\cos\theta+T(\psi_i,\Omega))]\sin\theta \\ =& -2\Re\{\overline{E}_2^{(p)}(\theta)\} \\ &\times [z_1+2z_2(\cos\theta+T(\psi_i,\Omega))]\sin\theta.\end{aligned} \tag{76}$$

By (76), it follows that the extrema should satisfy either $\Re\{\overline{E}_2^{(p)}(\theta)\} = 0$ or $[z_1+2z_2(\cos\theta+T(\psi_i,\Omega))]\sin\theta = 0$. Suppose that when $\theta=\theta_0$ we have $\Re\{\overline{E}_2^{(p)}(\theta_0)\}=0$. Then by (36), we can deduce that $|\overline{E}_2^{(p)}(\theta_0)|^2 \leq |\overline{E}_2^{(p)}(\theta)|^2$ for arbitrary $\theta \in [0^\circ, 360^\circ)$, i.e., θ_0 is a minimum. Thus, it suffices to consider the extrema that satisfy $[z_1+2z_2(\cos\theta+T(\psi_i,\Omega))]\sin\theta = 0$. In terms of $\frac{z_1}{2z_2}+T(\psi_i,\Omega) \in (-1,1)$, we have the following cases to consider:

1) $\frac{z_1}{2z_2}+T(\psi_i,\Omega) \in (-1,1)$. In this case, there are four extrema, $0^\circ, 180^\circ$ and $\theta = 180^\circ \pm \arccos(\frac{z_1}{2z_2}+T(\psi_i,\Omega))$, that satisfy $[z_1+2z_2(\cos\theta+T(\psi_i,\Omega))]\sin\theta = 0$. In order to guarantee the mainlobe orientation is at 0°, it suffices to ensure that $|\overline{E}_2^{(p)}(0^\circ)|^2 \geq |\overline{E}_2^{(p)}(180^\circ)|^2$ and $|\overline{E}_2^{(p)}(0^\circ)|^2 \geq |\overline{E}_2^{(p)}(180^\circ \pm \arccos(\frac{z_1}{2z_2}+T(\psi_i,\Omega)))|^2$. For $|\overline{E}_2^{(p)}(0^\circ)|^2 \geq |\overline{E}_2^{(p)}(180^\circ)|^2$, we have

$$-2z_2T(\psi_i,\Omega) \leq z_1 \leq 1/[1-T(\psi_i,\Omega)]. \tag{77}$$

Moreover, for $|\overline{E}_2^{(p)}(0^\circ)|^2 \geq |\overline{E}_2^{(p)}(180^\circ \pm \arccos(\frac{z_1}{2z_2}+T(\psi_i,\Omega)))|^2$, we obtain

$$\begin{aligned}&-2\sqrt{2z_2}-2z_2(1-T(\psi_i,\Omega)) \leq z_1 \\ &\leq 2\sqrt{2z_2}-2z_2(1-T(\psi_i,\Omega)).\end{aligned} \tag{78}$$

By (13), (77) and (78), we further have

1.1) For $T(\psi_i,\Omega) \geq 0$,

$$\begin{cases} 2\sqrt{z_2}-2z_2 \leq z_1 < 2z_2, & z_2 \in (1/4, 1/2) \quad (79a) \\ 2\sqrt{z_2}-2z_2 \leq z_1 \leq 2\sqrt{2z_2}-2z_2, & z_2 \in [1/2, 12-8\sqrt{2}) \quad (79b) \\ 2\sqrt{z_2}-2z_2 \leq z_1 < 2-3z_2/2, & z_2 \in \left[12-8\sqrt{2}, 1\right) \quad (79c) \\ 0 \leq z_1 < 2-3z_2/2, & z_2 \in [1, 4/3) \quad (79d) \end{cases}$$

1.2) For $\frac{3-\sqrt{2}-\sqrt{6-2\sqrt{2}}}{2} \leq T(\psi_i,\Omega) < 0$,

$$\begin{cases} 2\sqrt{z_2}-2z_2 \leq z_1 < 2z_2(1-T(\psi_i,\Omega)), \\ \qquad z_2 \in \left(\frac{1}{(2-T)^2}, \frac{1}{2(1-T(\psi_i,\Omega))^2}\right) & (80a) \\ 2\sqrt{z_2}-2z_2 \leq z_1 \leq 2\sqrt{2z_2}-2z_2(1-T(\psi_i,\Omega)), \\ \quad z_2 \in \left[\frac{1}{2(1-T(\psi_i,\Omega))^2}, \right. \\ \qquad \left. \frac{12+16T(\psi_i,\Omega)-8\sqrt{2+8T(\psi_i,\Omega)}}{(1-4T(\psi_i,\Omega))^2}\right) & (80b) \\ 2\sqrt{z_2}-2z_2 \leq z_1 < 2-3z_2/2, \\ \quad z_2 \in \left[\frac{12+16T(\psi_i,\Omega)-8\sqrt{2+8T(\psi_i,\Omega)}}{(1-4T(\psi_i,\Omega))^2}, \right. \\ \qquad \left. \frac{1}{(1-T(\psi_i,\Omega))^2}\right) & (80c) \\ -2z_2T(\psi_i,\Omega) \leq z_1 < 2-3z_2/2, \\ \qquad z_2 \in \left[\frac{1}{(1-T(\psi_i,\Omega))^2}, \frac{4}{(3-4T(\psi_i,\Omega))}\right) & (80d) \end{cases}$$

1.3) For $\frac{1-\sqrt{3}}{4} \leq T(\psi_i,\Omega) < \frac{3-\sqrt{2}-\sqrt{6-2\sqrt{2}}}{2}$,

$$\begin{cases} 2\sqrt{z_2}-2z_2 \leq z_1 < 2z_2(1-T(\psi_i,\Omega)), \\ \qquad z_2 \in \left(\frac{1}{(2-T(\psi_i,\Omega))^2}, \frac{1}{2(1-T(\psi_i,\Omega))^2}\right) & (81a) \\ 2\sqrt{z_2}-2z_2 \leq z_1 \leq 2\sqrt{2z_2}-2z_2(1-T(\psi_i,\Omega)), \\ \qquad z_2 \in \left[\frac{1}{2(1-T(\psi_i,\Omega))^2}, \frac{1}{(1-T(\psi_i,\Omega))^2}\right) & (81b) \\ -2z_2T \leq z_1 < 2\sqrt{2z_2}-2z_2(1-T), \\ \quad z_2 \in \left[\frac{1}{(1-T(\psi_i,\Omega))^2}, \right. \\ \qquad \left. \frac{12+16T(\psi_i,\Omega)-8\sqrt{2+8T(\psi_i,\Omega)}}{(1-4T(\psi_i,\Omega))^2}\right) & (81c) \\ -2z_2T(\psi_i,\Omega) \leq z_1 < 2-3z_2/2, \\ \quad z_2 \in \left[\frac{12+16T(\psi_i,\Omega)-8\sqrt{2+8T(\psi_i,\Omega)}}{(1-4T(\psi_i,\Omega))^2}, \right. \\ \qquad \left. \frac{4}{3-4T(\psi_i,\Omega)}\right) & (81d) \end{cases}$$

1.4) For $-\frac{\sqrt{2}}{2} \leq T(\psi_i,\Omega) < \frac{1-\sqrt{3}}{4}$,

$$\begin{cases} 2\sqrt{z_2}-2z_2 \leq z_1 < 2z_2(1-T(\psi_i,\Omega)) \\ \qquad z_2 \in \left(\frac{1}{(2-T(\psi_i,\Omega))^2}, \frac{1}{2(1-T(\psi_i,\Omega))^2}\right) & (82a) \\ 2\sqrt{z_2}-2z_2 \leq z_1 \leq 2\sqrt{2z_2}-2z_2(1-T(\psi_i,\Omega)), \\ \qquad z_2 \in \left[\frac{1}{2(1-T(\psi_i,\Omega))^2}, \frac{1}{(1-T(\psi_i,\Omega))^2}\right) & (82b) \\ -2z_2T(\psi_i,\Omega) \leq z_1 < 2\sqrt{2z_2}-2z_2(1-T(\psi_i,\Omega)), \\ \qquad z_2 \in \left[\frac{1}{(1-T(\psi_i,\Omega))^2}, \frac{2}{(1-2T(\psi_i,\Omega))^2}\right] & (82c) \end{cases}$$

1.5) For $-\sqrt{2} \leq T(\psi_i,\Omega) < -\frac{\sqrt{2}}{2}$,

$$\begin{cases} 2\sqrt{z_2}-2z_2 \leq z_1 < 2z_2(1-T(\psi_i,\Omega)), \\ \qquad z_2 \in \left(\frac{1}{(2-T(\psi_i,\Omega))^2}, \frac{1}{2(1-T(\psi_i,\Omega))^2}\right) & (83a) \\ 2\sqrt{z_2}-2z_2 \leq z_1 \leq 2\sqrt{2z_2}-2z_2(1-T(\psi_i,\Omega)), \\ \qquad z_2 \in \left[\frac{1}{2(1-T(\psi_i,\Omega))^2}, \frac{3-2\sqrt{2}}{T^2(\psi_i,\Omega)}\right] & (83b) \end{cases}$$

2) $\frac{z_1}{2z_2}+T(\psi_i,\Omega) \notin (-1,1)$. For this case, there only exist two extrema, i.e, 0° and 180°, that satisfy $[z_1+2z_2(\cos\theta+T(\psi_i,\Omega))]\sin\theta = 0$. To keep the mainlobe orientation at 0°, we require that $|\overline{E}_2^{(p)}(0^\circ)|^2 \geq |\overline{E}_2^{(p)}(180^\circ)|^2$, which can be equivalently expressed as

2.1) For $T(\psi_i,\Omega)\geq 0$,

$$\begin{cases} 2\sqrt{z_2}-2z_2\leq z_1\leq 1, & z_2\in(0,1/4) \quad (84a)\\ 2z_2(1-T(\psi_i,\Omega))\leq z_1\leq 1, & z_2\in[1/4,1/2] \quad (84b)\end{cases}$$

2.2) For $-\sqrt{2}\leq T(\psi_i,\Omega)<0$,

$$\begin{cases} 2\sqrt{z_2}-2z_2\leq z_1\leq 1/(1-T(\psi_i,\Omega)), \\ \qquad z_2\in\left(0,\dfrac{1}{(2-T(\psi_i,\Omega))^2}\right) \quad (85a)\\ 2z_2(1-T(\psi_i,\Omega))\leq z_1\leq 1/(1-T(\psi_i,\Omega)), \\ \quad z_2\in\left[\dfrac{1}{(2-T(\psi_i,\Omega))^2},\dfrac{1}{2(1-T(\psi_i,\Omega))^2}\right] \quad (85b)\end{cases}$$

2.3) For $T(\psi_i,\Omega)<-\sqrt{2}$,

$$2\sqrt{z_2}-2z_2\leq z_1\leq 1/(1-T(\psi_i,\Omega)),$$
$$z_2\in\left(0,\frac{\sqrt{2T(\psi_i,\Omega)-2T^3(\psi_i,\Omega)+T^4(\psi_i,\Omega)-1}}{2(1-T(\psi_i,\Omega))^2}+\frac{-T(\psi_i,\Omega)+T^2(\psi_i,\Omega)}{2(1-T(\psi_i,\Omega))^2}\right] \quad (86)$$

Finally, in order to simplify the results, we can merge (79) with (84), (80) with (85), (81) with (85), (82) with (85), and (83) with (85), which yield (38), (39), (40), (41) and (42), respectively. In addition, (86) leads directly to (43).

Now we analyze the case when (38)–(43) does not hold. In this case, the mainlobe orientation is either at $180^\circ\pm\arccos(z_1/(2z_2)+T(\psi_i,\Omega))$ or 180°. According to our previous analysis, for $\frac{z_1}{2z_2}+T(\psi_i,\Omega)\in(-1,1)$ there exist four extrema. If $z_1\geq 2\sqrt{2z_2[1+4z_2(1-T(\psi_i,\Omega))]}-2z_2(3-T(\psi_i,\Omega))$, then it follows that

$$|\overline{E}_2^{(p)}\left(180^\circ\pm\arccos\left(\frac{z_1}{2z_2}+T(\psi_i,\Omega)\right)\right)|^2\geq|\overline{E}_2^{(p)}(0^\circ)|^2 \quad (87)$$

$$|\overline{E}_2^{(p)}\left(180^\circ\pm\arccos\left(\frac{z_1}{2z_2}+T(\psi_i,\Omega)\right)\right)|^2\geq|\overline{E}_2^{(p)}(180^\circ)|^2. \quad (88)$$

It implies that the mainlobe is oriented toward $180^\circ\pm\arccos(z_1/(2z_2)+T(\psi_i,\Omega))$. Otherwise, i.e., if $z_1<2\sqrt{2z_2(1+4z_2(1-T(\psi_i,\Omega)))}-2z_2(3-T(\psi_i,\Omega))$, we obtain

$$|\overline{E}_2^{(p)}(180^\circ)|^2\geq|\overline{E}_2^{(p)}(0^\circ)|^2 \quad (89)$$

$$|\overline{E}_2^{(p)}(180^\circ)|^2\geq\left|\overline{E}_2^{(p)}\left(180^\circ\pm\arccos\left(\frac{z_1}{2z_2}+T(\psi_i,\Omega)\right)\right)\right|^2. \quad (90)$$

For $\frac{z_1}{2z_2}+T(\psi_i,\Omega)\notin(-1,1)$, there are two local maxima at $\theta=0^\circ$ and 180°. In this case, we have $|\overline{E}_2^{(p)}(180^\circ)|^2\geq|\overline{E}_2^{(p)}(0^\circ)|^2$, i.e., the mainlobe is also oriented toward 180°.

Appendix G
Proof of Proposition 7

To guarantee the mainlobe orientation of the second-order DMA is always at 0° with microphone gain errors $\eta_i\in[1-\Delta_\epsilon,1+\Delta_\epsilon]$, we have:

1) $G(\eta_i,\Omega)\geq 0$. For arbitrary z_1 and z_2, we can deduce that (27) always holds. Then according to Proposition 1, the mainlobe orientation of the second-order DMAs is always at 0°.

2) $G(\eta_i,\Omega)<0$. Taking the derivative of $G(\eta_i,\Omega)$ with respect to η_1,η_2,η_3 and Ω, respectively. For small microphone gain errors, we get $\frac{\partial G(\eta_i,\Omega)}{\partial\eta_1}=-\frac{1}{\eta_3\Omega^2}<0$, $\frac{\partial G(\eta_i,\Omega)}{\partial\eta_2}=\frac{2(2\eta_2-\eta_3)}{\eta_3^2\Omega^2}>0$, $\frac{\partial G(\eta_i,\Omega)}{\partial\eta_3}=\frac{\eta_3(\eta_1+2\eta_2)-4\eta_2^2}{\eta_3^2\Omega^2}<0$, $\frac{\partial G(\eta_i,\Omega)}{\partial\Omega}=-\frac{2G(\eta_i,\Omega)}{2\Omega}>0$, which indicate that $G(\eta_i,\Omega)$ is a decreasing function of η_1 and η_3, and is an increasing function of η_2 and Ω. Since $\eta_i\in[1-\Delta_\epsilon,1+\Delta_\epsilon]$ and $\Omega\in[\frac{2\pi d}{c}f_l,\frac{2\pi d}{c}f_h]\triangleq[\underline{\Omega},\overline{\Omega}]$, we have

$$G(\eta_i,\Omega)\in\left[-4\Delta_\epsilon(1-\Delta_\epsilon)/[(1+\Delta_\epsilon)^2\underline{\Omega}^2],0\right). \quad (91)$$

Accordingly, it follows that:

- To ensure that (64)–(67) hold, by substituting (91) into (64)–(67), we can deduce the tolerance of microphone gain errors Δ_ϵ should satisfy $\Delta_\epsilon\leq\frac{c^2+2\pi^2f_l^2d^2X-c\sqrt{c^2+8\pi^2f_l^2d^2X}}{2(c^2-\pi^2f_l^2d^2X)}$ with $\frac{z_1}{2z_2}\in(-1,1)$, where $X=[(z_1+2z_2)^2-8z_2]/(8z_2^2)$.
- Otherwise, to ensure that (70) and (71) hold, by substituting (91) into (70) and (71), we can obtain the tolerance of microphone gain errors Δ_ϵ should satisfy $\Delta_\epsilon\leq\frac{c^2+2\pi^2f_l^2d^2Y-c\sqrt{c^2+8\pi^2f_l^2d^2Y}}{2(c^2-\pi^2f_l^2d^2Y)}$ with $\frac{z_1}{2z_2}\notin(-1,1)$, where $Y=(z_1-1)/z_2$.

Appendix H
Proof of Proposition 8

To ensure the mainlobe orientation of the second-order DMA is always at 0° with microphone phase errors $\psi_i\in[-\Delta_\psi,\Delta_\psi]$, we have:

1) $T(\psi_i,\Omega)\geq 0$. For small microphone phase errors, we can deduce from Proposition 1 that (38) holds, for an arbitrary z_1 and z_2, which implies that the mainlobe orientation of the second-order DMAs is always at 0°.

2) $T(\psi_i,\Omega)<0$. Define $\chi_2=\psi_2-\psi_3$. Then $T(\psi_i,\Omega)$ can be reformulated as $T(\psi_i,\Omega)=\frac{\chi_2}{\Omega}$. Taking the derivative of $T(\psi_i,\Omega)$ with respect to χ_2 and Ω, respectively. We have $\frac{\partial T(\psi_i,\Omega))}{\partial\chi_2}=\frac{1}{\Omega}>0$ and $\frac{\partial T(\psi_i,\Omega))}{\partial\Omega}=-\frac{\chi_2}{\Omega^2}>0$, i.e., $T(\psi_i,\Omega)$ is an increasing function of χ_2 and Ω. Reconsidering that $\psi_i\in[-\Delta_\psi,\Delta_\psi]$, $\Omega\in[\frac{2\pi d}{c}f_l,\frac{2\pi d}{c}f_h]\triangleq[\underline{\Omega},\overline{\Omega}]$, we get

$$T(\psi_i,\Omega)\in[-2\Delta_\psi/\underline{\Omega},0). \quad (92)$$

Accordingly, we further have

- To ensure that (85) and (86) hold, by substituting (92) into (85) and (86), we get the tolerance of microphone phase errors $\Delta_\psi\leq\frac{\pi f_l d(1-z_1)}{cz_1}$ with $\frac{z_1}{2z_2}+T(\psi_i,\Omega)\notin(-1,1)$, or equivalently, with $z_1^2-2z_2+4z_1z_2\leq 0$ or $z_1\geq\sqrt{2z_2}$.
- Otherwise, to ensure (80)–(83) hold, by substituting (92) into (80)–(83), we get $\Delta_\psi\leq\frac{\pi f_l d(\sqrt{8z_2}-2z_2-z_1)}{2cz_2}$ or $\Delta_\psi\leq\frac{\pi f_l dz_1}{2cz_2}$ with $\frac{z_1}{2z_2}+T(\psi_i,\Omega)\in(-1,1)$, or equivalently, with $\sqrt{2z_2}-2z_2<z_1<\sqrt{2z_2}$. Therefore, the tolerance of microphone phase errors should satisfy $\Delta_\psi\leq\min\{\frac{\pi f_l d(\sqrt{8z_2}-2z_2-z_1)}{2cz_2},\frac{\pi f_l dz_1}{2cz_2}\}$ with $\sqrt{2z_2}-2z_2<z_1<\sqrt{2z_2}$.

REFERENCES

[1] G. W. Elko, "Differential microphone arrays," in *Audio Signal Processing for Next-Generation Multimedia Communication Systems*, Y. Huang and J. Benesty, Eds. Boston, MA, USA: Springer, 2004, ch. 2, pp. 11–65.

[2] G. W. Elko and A. T. N. Pong, "A simple first-order differential microphone," in *Proc. Workshop Appl. Signal Process. Audio Acoust.*, 1995, pp. 169–172.

[3] G. W. Elko and A. T. N. Pong, "A steerable and variable first-order differential microphone array," in *Proc. Int. Conf. Acoust., Speech, Signal Process.*, 1997, pp. 223–226.

[4] H. Teutsch and G. W. Elko, "First- and second-order adaptive differential microphone arrays," in *Proc. Int. Workshop Acoust. Echo Noise Control*, 2001, pp. 35–38.

[5] M. Buck, "Aspects of first-order differential microphone arrays in the presence of sensor imperfections," *Eur. Trans. Telecomm.*, vol. 13, pp. 115–122, 2002.

[6] F. Talantzis, A. G. Constantinides, and L. C. Polymenakos, "Using a differential microphone array to estimate the direction of arrival of two acoustic sources," in *Proc. INTERSPEECH*, 2006, pp. 2602–2605.

[7] B. Gunel, H. Hacihabiboğlu, and A. M. Kondoz, "Acoustic source separation of convolutive mixtures based on intensity vector statistics," *IEEE Trans. Audio, Speech, Lang. Process.*, vol. 16, no. 4, pp. 748–756, May 2008.

[8] G. W. Elko and J. Meyer, "Second-order differential adaptive microphone array," in *Proc. Int. Conf. Acoust., Speech, Signal Process.*, 2009, pp. 73–76.

[9] R. M. M. Derkx and K. Janse, "Theoretical analysis of a first-order azimuth-steerable superdirective microphone array," *IEEE Trans. Audio, Speech, Lang. Process.*, vol. 17, no. 1, pp. 150–162, Jan. 2009.

[10] T. D. Abhayapala and A. Gupta, "Higher order differential-integral microphone arrays," *J. Acoust. Soc. Amer.*, vol. 127, pp. EL227–EL233, 2010.

[11] M. Kolundzija, C. Faller, and M. Vetterli, "Spatiotemporal gradient analysis of differential microphone arrays," *J. Audio Eng. Soc.*, vol. 59, pp. 20–28, 2011.

[12] E. De Sena, H. Hacihabiboğlu, and Z. Cvetković, "On the design and implementation of higher order differential microphones," *IEEE Trans. Audio, Speech, Lang. Process.*, vol. 20, no. 1, pp. 162–174, Jan. 2012.

[13] J. Benesty, M. Souden, and Y. Huang, "A perspective on differential microphone arrays in the context of noise reduction," *IEEE Trans. Audio, Speech, Lang. Process.*, vol. 20, no. 2, pp. 699–704, Feb. 2012.

[14] J. Benesty and J. Chen, *Study and Design of Differential Microphone Arrays*. Berlin, Germany: Springer, 2013.

[15] L. Zhao, J. Benesty, and J. Chen, "Design of robust differential microphone arrays," *IEEE/ACM Trans. Audio, Speech, Lang. Process.*, vol. 22, no. 10, pp. 1455–1465, Oct. 2014.

[16] X. Wu, H. Chen, J. Zhou, and T. Guo, "Study of the mainlobe misorientation of the first-order steerable differential array in the presence of microphone gain and phase errors," *IEEE Signal Process. Lett.*, vol. 21, no. 6, pp. 667–671, Jun. 2014.

[17] C. Pan, J. Chen, and J. Benesty, "Theoretical analysis of differential microphone array beamforming and an improved solution," *IEEE/ACM Trans. Audio, Speech, Lang. Process.*, vol. 23, no. 11, pp. 2093–2105, Nov. 2015.

[18] L. Zhao, J. Benesty, and J. Chen, "Design of robust differential microphone arrays with the Jacob-Anger expansion," *Appl. Acoust.*, vol. 110, pp. 194–206, 2016.

[19] X. Wu and H. Chen, "Directivity factors of the first-order steerable differential array with microphone mismatches: Deterministic and worst-case analysis," *IEEE/ACM Trans. Audio, Speech, Lang. Process.*, vol. 24, no. 2, pp. 300–315, Feb. 2016.

[20] G. Huang, J. Benesty, and J. Chen, "Design of robust concentric circular differential microphone arrays," *J. Acoust. Soc. Amer.*, vol. 141, pp. 3236–3249, 2017.

[21] A. Bernardini, M. D'Aria, R. Sannino, and A. Sarti, "Efficient continuous beam steering for planar arrays of differential microphones," *IEEE Signal Process. Lett.*, vol. 24, no. 6, pp. 794–798, Jun. 2017.

[22] Y. Buchris, I. Cohen, and J. Benesty, "Frequency-domain design of asymmetric circular differential microphone arrays," *IEEE/ACM Trans. Audio, Speech, Lang. Process.*, vol. 26, no. 4, pp. 760–773, Apr. 2018.

[23] A. Bernardini, F. Antonacci, and A. Sarti, "Wave digital implementation of robust first-order differential microphone arrays," *IEEE Signal Process. Lett.*, vol. 25, no. 2, pp. 253–257, Feb. 2018.

[24] M. Buck and M. Rößler, "First order differential microphone arrays for automotive applications," in *Proc. Int. Workshop Acoust. Echo Noise Control*, 2001, pp. 19–22.

[25] M. Ihle, "Differential microphone arrays for spectral subtraction," in *Proc. Int. Workshop Acoust. Echo Noise Control*, 2003, pp. 259–262.

[26] A. Álvarez, P. Gómez, R. Martínez, V. Rodellar, and V Nieto, "Speech enhancement for a car environment support by a first-order differential microphone," in *Proc. EUSIPCO*, 2004, pp. 1955–1958.

[27] H. Song and J. Liu, "First-order differential microphone array for robust speech enhancement," in *Proc. Int. Conf. Audio, Lang. Image Process.*, 2008, pp. 1461–1466.

[28] H. Puder, E. Fischer, and J. Hain, "Optimized directional processing in hearing aids with integrated spatial noise reduction," in *Proc. Int. Workshop Acoust. Echo Noise Control*, 2012, pp. 1–4.

[29] X. Wu and H. Chen, "Design and analysis of second-order steerable differential microphone arrays," in *Proc. EUSIPCO*, 2017, pp. 1245–1249.

[30] J. Byun, Y. C. Park, and S. W. Park, "Continuously steerable second-order differential microphone arrays," *J. Acoust. Soc. Amer.*, vol. 143, pp. EL225–EL230, 2018.

[31] S. He and H. Chen, "Closed-form DOA estimation using first-order differential microphone arrays via joint temporal-spectral-spatial processing," *IEEE Sensors J.*, vol. 17, no. 4, pp. 1046–1060, Feb. 2017.

[32] S. Ding and H. Chen, "DOA estimation of multiple speech sources by selecting reliable local sound intensity estimates," *Appl. Acoust.*, vol. 127, pp. 336–345, 2017.

[33] X. Chen, W. Wang, Y. Wang, X. Zhong, and A. Alinaghi, "Reverberant speech separation with probabilistic time-frequency masking for B-format recordings," *Speech Commun.*, vol. 68, pp. 41–54, 2015.

[34] [Online]. Available: https://www.invensense.com/wp-content/uploads/2016/05/AN-000056-v1.0.pdf, Accessed on: Aug. 2019.

[35] [Online]. Available: https://www.knowles.com/docs/default-source/default-document-library/frequency-response-and-latency-of-mems-microphones--theory-and-practice.pdf?sfvrsn=4, Accessed on: Aug. 2019.

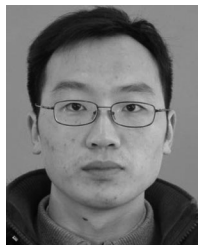

Quansheng Tu received the B.S. and M.S. degrees from Anhui Normal University, Wuhu, China, in 2012 and 2015, respectively. He is currently working toward the Ph.D. degree in communication and information systems with the Nanjing University of Aeronautics and Astronautics, Nanjing, China. His research interests include sensor array signal processing and acoustical signal processing.

Huawei Chen was born in Henan, China, in 1977. He received the B.S. degree from Henan Normal University, Xinxiang, China, in 1999, and the M.S. and Ph.D. degrees from Northwestern Polytechnical University, Xian, China, in 2002 and 2004, respectively.

In 2004, he joined the Department of Electronic Science and Engineering and the Institute of Acoustics, Nanjing University, Nanjing, China, as a Postdoctoral Researcher. From August 2005 to August 2009, he was with the Centre for Signal Processing, School of Electrical and Electronic Engineering, Nanyang Technological University, Singapore, as a Research Fellow. Since September 2009, he has been a Professor with the College of Electronic and Information Engineering, Nanjing University of Aeronautics and Astronautics, China. He has authored or coauthoed more than 90 research papers in refereed journals and conferences. His current research interests include microphone array signal processing, acoustical and speech signal processing, statistical and adaptive signal processing. He is currently an Associate Editor for the journal IEEE ACCESS and the Springer journal *Circuits, Systems, and Signal Processing*.